Investigations on inner Structures of the Propeller Blade referring Additive Manufacturin

Auteur : Saeed, Muthair
Promoteur(s) : Rigo, Philippe
Faculté : Faculté des Sciences appliquées
Diplôme : Master : ingénieur civil mécanicien, à finalité spécialisée en "Advanced Ship Design"
Année académique : 2024-2025
URI/URL : http://hdl.handle.net/2268.2/25050

Investigations on Inner Structures of the Propeller Blade referring to Additive Manufacturing

by Muthair Saeed

muthair.saeed@uni-rostock.de

Student ID No.: 224202273

First Reviewer:

Dr.-Eng. Patrick Kaeding

patrick.kaeding@uni-rostock.de

Professor Uni-Rostock/ Hiroshima Uni.

University of Rostock

18059 Rostock. Germany

Second Reviewer:

Dipl.-Eng. Jörn Klüss

development@mmg-propeller.de

Head of Design Department

Mecklenburger Metallguss GmbH (MMG)

D-17192 Waren (Müritz), Germany

EMship+ Advanced Design

Master Thesis

Investigations on Inner Structures of the Propeller Blade referring to Additive Manufacturing

© Muthair Saeed.

All work in this thesis was carried out in:

Mecklenburger Metallguss GmbH

Teterower Str. 1

D-17192 Waren (Müritz),

Germany

Faculty Supervisor: Dr.-Eng./Hiroshima Uni. Patrick Kaeding (University of Rostock, Germany), Dipl.-Ing. Gunnar Kistner (University of Rostock, Germany)

Direct Supervisor: Dipl.-Eng. Jörn Klüss (MMG, Gemany)

Restriction notice

The submitted master's thesis entitled:

Investigations on Inner Structures of the Propeller Blade referring to Additive Manufacturing.

This document contains confidential and internal data belonging to the company

Mecklenburger Metallguss GmbH (MMG)

Teterower Straße 1

17192 Waren (Müritz)

Unauthorised persons are not permitted to view the master's thesis. Exceptions to this rule are the reviewers and authorised members of the examination board. The reproduction and publication of the thesis, even in excerpts, is strictly prohibited.

Some data have been removed because of Confidentiality

Any exceptions to this rule require the approval of the above-mentioned.

Declaration of Authorship

I declare that this thesis and the work presented in it are my own and have been generated by me as the result of my own original research. Where I have consulted the published work of others, this is always clearly attributed. Where I have quoted from the work of others, the source is always given. With the exception of such quotations, this thesis is entirely my own work. I have acknowledged all main sources of help. Where the thesis is based on work done by myself jointly with others, I have made clear exactly what was done by others and what I have contributed myself. This thesis contains no material that has been submitted previously, in whole or in part, for the award of any other academic degree or diploma.

I cede copyright of the thesis in favour of the University of Rostock.

Rostock, July 31, 2025

………………………….

Muthair Saeed

Acknowledgement

I would like to express my deepest gratitude to my supervisor at MMG, Mr. Jörn Klüss, whose unwavering support, guidance, and expertise have been instrumental throughout the course of this thesis. His willingness to share his profound knowledge of structure design and his constant encouragement greatly enriched my learning experience and helped shape the direction of this research.

My sincere thanks also go to the entire Research and Development department at MMG. Their openness, technical insights, and continuous support provided a highly collaborative environment in which I was able to develop and refine my ideas effectively.

I am equally grateful to my academic supervisor, Prof. Patrick Kaeding, and to Mr. Gunnar Kistner for their valuable feedback, constructive suggestions, and continued guidance throughout the academic supervision of this work.

Finally, I extend my heartfelt appreciation to the entire EMSHIP+ team for offering such a unique and enriching academic opportunity. This program has not only broadened my technical perspective but also allowed me to work within an international, multidisciplinary framework that has deeply shaped my professional development.

CONTENTS

List of Figures:

List of Tables:

List of Graphs:

ABSTRACT

Propeller blades in maritime propulsion systems must withstand complex hydrodynamic loads, torsional stresses, cavitation, and varying static and dynamic pressures, while delivering high thrust, torque, and efficiency. Traditional manufacturing methods (casting and milling) limit designers to solid geometries, precluding the use of advanced hollow or lattice internal structures that reduce weight and material usage. These limitations are overcome by additive manufacturing (AM), especially Wire Arc Additive Manufacturing (WAAM), which makes it possible to produce complex, lightweight designs with integrated internal features in a near-net-shape. In this work, unique internal configurations, derived via topology optimization and biomimetic patterns (honeycomb, gyroid, and bone-inspired lattices), are investigated for propeller blades operating in diverse environments, from open water to ice-prone seas. Emphasis is placed on selecting suitable AM materials (e.g., high-nickel aluminum bronze) and on developing robust WAAM-milling hybrid processes to ensure consistent bead geometry, material integrity, and compliance with DNV certification guidelines. Finite element analyses validate that optimized internal structures, in which different configurations of internal structures achieve favorable stiffness-to-mass ratios while respecting fatigue and strength criteria. This research outlines both design methodologies and manufacturing parameters necessary to realize next-generation, additively manufactured marine propellers.

This page is left blank intensionally.

1. INTRODUCTION:

Propellers are critical components in the maritime propulsion system since they are responsible for propelling and maneuvering the vessel, which is done by accelerating water around the blades and transforming the rotational energy into thrust. A number of factors, including thrust, torque, and efficiency, affect how well they perform. In order to withstand resilience in complex hydrodynamic loads produced by torsional stresses, cavitation, and static and dynamic pressures, propellers are frequently constructed from high-strength alloys such as nickel-aluminum bronze or stainless steel. Their structural complexity is constrained because of traditional production techniques like casting and milling, which frequently produce a solid part in a single piece. While using the advanced internal structures, which could improve performance while using less material and energy, is very difficult to achieve using these approaches.

To fix this issue, a modern manufacturing technique like Additive manufacturing can be used. Additive manufacturing (AM) has emerged as a transformative technology that enables the production of intricate and lightweight designs that were previously unattainable. This technology can be used for propeller manufacturing as it allows rapid prototyping, along with customization for specialized vessels, and the ability to integrate hollow internal structures. Such designs can significantly reduce weight and material waste, which also aligns with global sustainability goals. This method also involves the selection of suitable material for the AM process, as the layer strength highly depends on the selected material. However, optimizing these hollow structures requires meticulous consideration of operational loads and operational conditions, such as inhomogeneous hydrodynamic forces, rotational stresses, maneuver-induced strains, and ice-impact loads, etc., which should be within design limits to ensure structural integrity.

In this project, unique inner structures for propeller blades that are suitable for different vessel operating environments, from open-water navigation to the areas that are prone to ice, will be investigated and chosen. Research is concentrated on typology optimization and integration of biomimetic structures, such as honeycomb, gyroid, and trabecular bone-inspired structures, etc., which imitate naturally occurring evolutionary solutions for striking a balance between strength and weight by utilizing AM's design freedom. Along with design of internal structure this research will also focuses on manufacturing parameters required for these internal structure.

This page is left blank intensionally.

Chapter # 1

Detailed Study and Literature Review

1. BASICS OF PROPELLER DESIGN:

1.1. Propeller Geometry:

The main purpose of propeller is to accelerate the water around it to move the vessel forward. For analyzing the flow created by the moving propeller, it's important to understand the different parameters of propeller that led to the production of Thrust and efficiency. The main geometric parameters are shown in Figure 1.

(a) Pitch, Skew & Rake

(b) Blade section
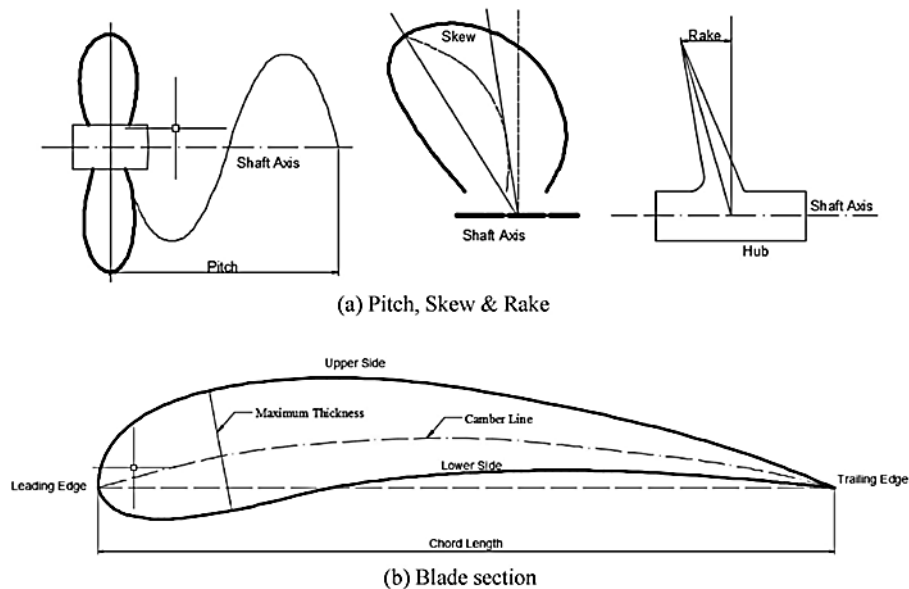
Figure 1 Propellor design parameters

Pitch: It's the distance propeller would move forward in one full rotation in case of no slip.

Skew: The angle by which the propeller blades are curved backward to reduce vibrations and improve efficiency.

Rake: The tilt of the propeller blades either forward or backward from the hub, affecting pressure excitations.

Chord Length: The straight-line distance from the leading edge to the trailing edge.

Camber Line: The curved line running along the center of a blade section, influencing lift and performance.

1.2. Design Parameters:

The design of a propeller is based on several factors, including ship dimensions, power, desired speed, operating conditions, ship resistance, and wake field etc. These factors are analyzed in detail and discussed below.

1.2.1. Hydrodynamic parameters in open water:

Figure 2 shows propeller properties in open water conditions, which refer to conditions without the influence of the ship wake.
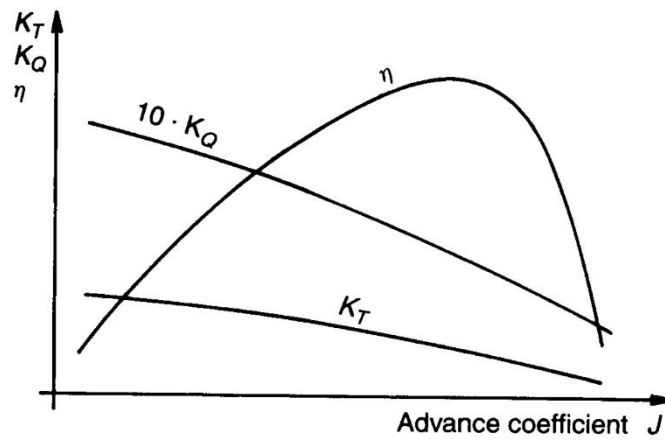
Figure 2 Propeller properties in open water (Kornev, 2019)

Propeller efficiency (ETAO): The ratio of useful power (thrust) to the input power (shaft power). It indicates how effectively a propeller converts engine power into thrust. It typically increases with **J** up to an optimal point, after which it decreases due to increased slip and reduced thrust effectiveness

Advance coefficient J: A dimensionless number representing the relationship between the ship's speed, including wake effect, and the propeller's rotational speed.

$$J = \frac{V_A}{n \times D} \tag{1}$$

Thrust Coefficient K_T: It's defined as the thrust normalized by the dynamic pressure and propeller dimensions. As J increases, the effective angle of attack of the blades reduces, leading to a decrease in thrust produced per revolution. In short, higher advance ratios generally result in a lower K_T.

$$K_T = \frac{T}{(\rho * n^2 * D^4)} \tag{2}$$

Torque Coefficient K_Q: It represents the torque required to drive the propeller, normalized similarly. With increasing J, the flow conditions change such that the torque needed to overcome fluid resistance typically declines. However, the K_Q curve is often more complex; it may exhibit a peak at lower J when propeller just starts to accelerate the water, and it falls off as J increases further.

$$K_Q = \frac{Q}{(\rho * n^2 * D^5)} \tag{3}$$

1.2.2. Influence of Diameter and Pitch:

To check the influence of propeller diameter (D) and pitch-to-diameter ratio (P/D) on shaft power and propeller speed, an 80,000-dwt vessel is considered. The graph between shaft power and propeller speed is given in Graph 1.
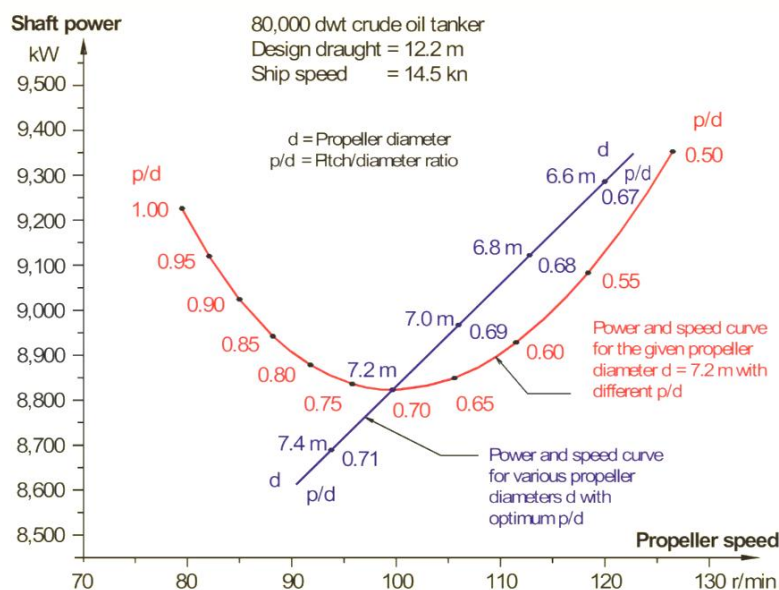
Graph 1 Influence of Diameter and Pitch on Propeller Design (Basic Principles of Ship Propulsion, MAN Diesel & Turbo.no date)

Red Curve (Fixed Diameter, Varying P/D)

- Represents the required shaft power for a **fixed propeller diameter (D = 7.2 m)** with different **pitch-to-diameter ratios (P/D)**.

- Higher **P/D** (e.g., 1.0) results in lower propeller speed and higher power demand.

- Lower **P/D** (e.g., 0.5) increases propeller speed but requires more power.

Blue Curve (Optimal P/D for Different Diameters)

- Shows shaft power requirement for various (**D**) with their optimal **P/D** values.

- Larger diameters (e.g., **7.4 m**) operate at lower speeds and require less power.

- Smaller diameters (e.g., **6.6 m**) operate at higher speeds but demand more power.

So, it's clear from the graph that larger propellers with optimal P/D are more efficient as they require less shaft power for the same thrust, and higher P/D values increase power demand but reduce propeller speed. So, choosing the right combination of d and P/D is crucial for fuel efficiency and performance. Click or tap here to enter text.

1.2.3. *Influence of ship resistance and continuous service on Power:*

To analyze how different types of ship resistance (e.g., hull fouling, weather conditions, sea margins) influence the continuous service rating of a marine propulsion system. Propeller performance curves are compared under varying operational scenarios (clean vs. fouled hull, calm vs. heavy weather) and mapped against engine shaft power requirements relative to the Specified MCR (Maximum Continuous Rating). The main purpose of this analysis is to visualize how power demands shift under real-world conditions, ensuring optimal engine and propeller design for efficiency and reliability.
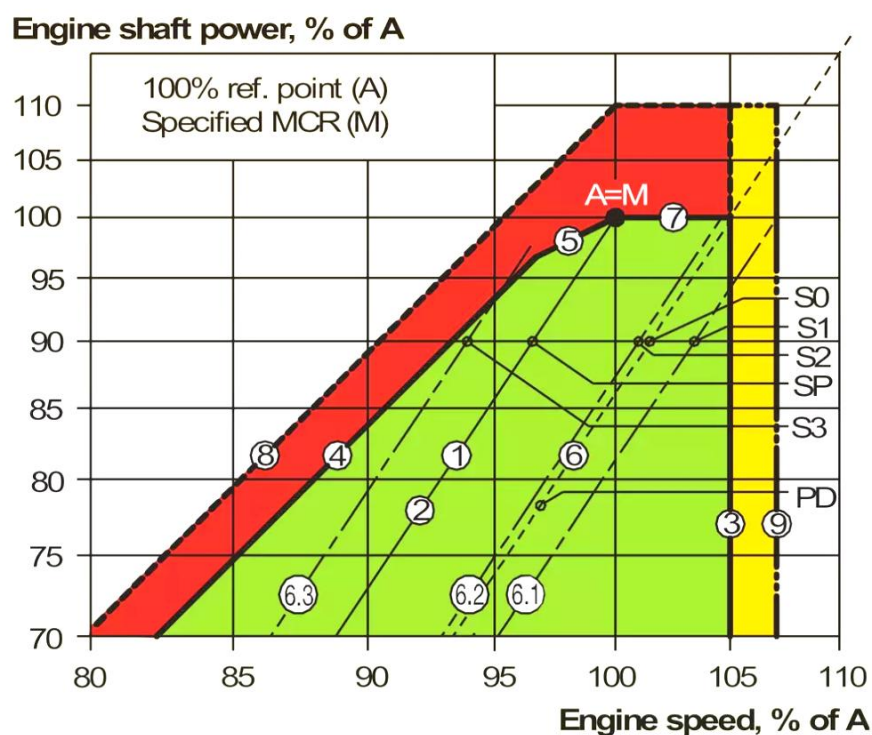
Graph 2 Influence of different type of ship resistance (*basis-propulsion.pdf*, no date)

Represents the engine's Maximum Continuous Rating (100% power and speed) that aligns with the ship's specification.

1. **Operational Scenarios (Resistance Types):**

   o **S0**: Clean hull, calm weather, loaded ship (baseline condition).

   o **S1**: Clean hull, calm weather, ballast (trial condition).

   o **S2**: Clean hull + 15% sea margin, loaded ship.

   o **SP**: Fouled hull, heavy weather, loaded ship.

   o **S3**: Very heavy sea and wave resistance.

2. **Propeller Curves:**

   o **Line 1**: Propeller curve through point **A=M** (Specified MCR point).

   o **Line 2**: Heavy propeller curve (fouled hull + heavy weather).

   o **Line 6**: Light propeller curve (clean hull + calm weather).

   o **Line 6.1:** Propeller curve for loaded ship with clean hull in calm weather condition.

   o **Line 6.2:** Propeller curve for ballast trial with clean hull in calm weather condition with 15% sea margin.

   o **Line 6.3:** Propeller curve for very heavy sea conditions and wave resistance.

3. **Engine Shaft Power vs. Specified MCR (%):**

   o **100% Reference Point (A)**: Specified MCR (baseline power).

   o **PD (Propeller Design Point)**: Corresponds to 80% power under clean hull/calm weather.

4. **Critical Observations:**

   o Power demand increases significantly under fouled hull/heavy weather (**SP**) and extreme seas (**S3**).

   o Clean hull/calm weather (**S0/S1**) requires lower power (e.g., 80% at PD).

   o The **15% sea margin (S2)** introduces moderate power adjustments.

All these different loading conditions have to be considered while designing the propeller.

1.3. Operation in behind condition and Load fluctuation at blade:

The load fluctuations at propeller blade are driven by complex hydrodynamic and mechanical interactions. As the propeller is located at stern part of vessel which rise to factors like wake effect and suction effect lead to variation in thrust and torque value. All these variations directly

impact the propeller's performance, structural integrity, and efficiency. The detail of these loads are given below.

1.3.1. *Hydrodynamic Factors Causing Load Fluctuations:*

- **Wake Field Variations**:

The propeller operates in the **non-uniform wake field** behind the ship's hull. As water flows unevenly around the hull because of the boundary layer, which creates a no-slip boundary condition around the hull. Therefore, the propeller blades experience cyclical changes in inflow velocity and angle, leading to **dynamic load variations**. Example: A blade passing through a high-wake region (e.g., near the hull) faces higher resistance than in a low-wake region.

- **Suction effect**:

The suction effect at the propeller directly influences thrust deduction by altering the hydrodynamic forces acting on the hull and propeller because, as the propeller rotates, it accelerates water backward to generate thrust. This creates a low-pressure region (suction) near the propeller disc, which "pulls" the surrounding water (and the ship's hull) forward.

The pressure distribution near the ship's stern is altered by the suction effect. Because the low-pressure area creates drag, this raises the effective resistance the hull encounters. The propeller must generate more push than is ostensibly required to move the ship forward in order to overcome this additional resistance. Thrust deduction (t) is the difference between the actual thrust produced by the propeller and the effective thrust needed, which is quantified as:

$$t = \frac{T - T_{effective}}{T} \tag{4}$$

where T = propeller thrust, $T_{effective}$ = thrust overcoming ship resistance.

- **Cavitation**: Lower pressure conditions on the blade surface can cause cavitation (formation and collapse of vapor bubbles). This creates impulsive loads, leading to vibrations, noise, and potential material erosion.

- **Maneuvering Operations**: During turns, acceleration, or deceleration, the propeller experiences rapid changes in thrust demand, causing transient load spikes or drops.

- **Environmental Conditions**: Waves, currents, and ice navigation introduce unsteady hydrodynamic forces, forcing the propeller to operate under fluctuating torque and thrust.

1.3.2. Operational Factors Influencing Blade Loads:

Engine Power Modulation: Changes in engine RPM or power output (e.g., to comply with speed limits or optimize fuel efficiency) alter the propeller's rotational speed, affecting blade loading.

Ship Loading Conditions: Ship in ballast (lighter) sits higher in the water, altering the propeller's immersion depth and hydrodynamic loading. On otherside biofouling increases hull resistance, forcing the propeller to work harder to maintain speed, leading to sustained higher loads.

Sea Margins and Weather: Operating with a **15% sea margin** (extra power reserve) or in heavy weather increases resistance, requiring the propeller to generate more thrust, which amplifies blade stresses.

All these load fluctuationled led to fatigue failure which is cause by inadequate design concerning increased loading conditions which leads to micro cracks, and at the end results in blade failure over time, so for propeller design all the loads have to be taken in account. On the other hand, the load imbalances cause vibrations that propagate through the shaft and hull, risking component wear and crew discomfort.

2. MAIN CLASSIFICATION RULES AND GUIDELINES:

The process of shipbuilding is followed by comprehensive and firm regulations defined by different Classification societies. These classification bodies guarantee that shipbuilders follow strict regulations in accordance with globally accepted standards throughout the design and construction phases. As these regulations are implemented after detailed studies to ensure the safety of the crew and ship during operation. A vessel is only permitted to operate after a thorough inspection and certification by the classification society, which is also necessary for processing insurance and other essential documentation.

There are different classification societies around the world. Some of the most important are Lloyd's Register (LR), Det Norske Veritas (DNV), Bureau Veritas (BV), Registro Italiano Navale (RINA), and the American Bureau of Shipping (ABS). In this project Det Norske Veritas (DNV) regulations are followd for propeller design and production.

2.1. Propeller Design and Documentation

Design Scope & Components:

- The design rules apply to propellers used for propulsion, steering, and maneuvering.
- All major parts (blades, blade fitting mechanisms, hub design) must be defined and approved.

Documentation Requirements:

- Detailed assembly and drawing documentations are required from the manufacturer which including geometry, material specifications, and heat treatment data.
- Designers must provide load-carrying details such as blade flange geometry, tolerance classes (e.g. per ISO 484), and information on weight, buoyancy, and mass moments of inertia.

Design Analysis:

- A comprehensive design analysis must include both conventional calculations and, for special designs, direct assessment by CFD and finite element (FE) methods.
- The documentation should verify that all components (including fittings and hub attachments) sustain operational and dynamic loads.

(See DNV-RU-SHIP Pt.4 Ch.5 for detailed propeller design requirements)

2.2. Propeller Blade Load & Stress Analysis per DNV Rules

2.2.1. High Cycle (Fatigue) Analysis:

− Stresses are assessed using both traditional formulas and advanced methods (CFD and FE simulations) to capture the dynamic nature of loading.

− The traditional formula for high-cycle stress criterion is written as:

$$S < \frac{U_1 K_{thick} - U_2 \sigma_m}{\sigma_m K_{str} M_t} \tag{5}$$

− S = safety factor.

− U_1 = high cycle fatigue strength amplitude [N/mm2] at zero mean stress.

− K_{str} = Load correction factor for adjusting the fluctuating nature of the blade loads, referring to the variation of the local blade stresses.

− K_{thick} = correction factor for the influence of wall thickness on fatigue strength.

− U_2 = Relative reduction of fatigue strength with increasing mean stress

− M_t = fluctuating load relative to the mean load.

− σ_m = actual mean stress.

− Some other factors include:

   ▪ Skew Correction Factor: Account for geometric influences on stress distribution.

   ▪ Bending Moment and Section Modulus Coefficients: Help determine effective resistance to bending.

− Centrifugal forces are also evaluated as part of the overall stress state.

(DNV-RU-SHIP Pt Ch 5-2.4.2):

2.2.2. Low Cycle Stress Assessment:

− Focuses on peak stress zones by considering sudden load changes and shock effects during operations such as start/stop or pitch adjustments.

2.2.3. Direct Assessment Methods:

− For complex or innovative designs, full CFD and FE analyses are recommended to verify that the blades can withstand both cyclic and transient loads.

– Such detailed simulations support the classification process by providing a clear picture of fatigue strength and structural behavior.

(Detailed calculation guidelines and correction factors are provided in DNV-CG-0039 "Calculation of Marine Propellers")

2.3. Propeller Strength Calculation (Additive Manufacturing)

For both general AM and WAAM processes, the strength calculation of propeller blades relies heavily on understanding the loads imposed during operation, such as hydrodynamic thrust, centrifugal forces, and torque. Propellers must be subjected to structural integrity analysis, regardless of the production technique, according to the DNV criteria. This often means comparing the material's fatigue and yield limitations with the pressures and bending moments caused by dynamic loads.

In WAAM-specific cases, because the process builds the part layer-by-layer using wire feedstock and arc welding, additional attention is given to residual stresses from the heat input and cooling cycles. More thorough non-destructive testing (NDT) and post-processing (such as heat treatment or hot isostatic pressing) may be necessary for WAAM-printed propellers in order to reduce stress and uniformize the material's characteristics.

WAAM-produced propellers still follow traditional design and load calculation rules found in DNV-CG-0039 (for strength and fatigue analysis), but additional checks are introduced due to the unique microstructures and possible anisotropy (layer-by-layer buildup) associated with the WAAM process.

2.4. General guidelines for Additive Manufacturing

According to DNV's classification standards, all propellers, including those made by standard AM or WAAM (Wire Arc Additive Manufacturing), must meet specific criteria for approval. This includes submission of comprehensive documentation on material specifications, load analysis, blade thickness determination, and fitting details. DNV-RU-SHIP Pt.4 Ch.5 defines the core requirements for rotating machinery and propellers, stating that both the hub and blades (fixed or controllable pitch) are subject to certification. Propellers are further required to comply with inspection regimes involving dimensional checks, NDT, and proof of fatigue resistance.

The approval procedure for manufacturers is described in DNV-CP-0267 for AM, and it calls for documented proof of the production controls, material traceability, and process route. The DNV-CG-0197 qualification frameworks, which include verifying process parameters (such as heat input and build strategy) and ensuring conformity with conventional propeller manufacturing standards, must be met by both general AM and WAAM processes.

3. PROPELLER MATERIAL AND BLADE THICKNESS:

Propeller materials must satisfy stringent criteria to ensure they can withstand the harsh marine environment while delivering reliable performance. The detailed overview of classification society rules regarding propeller material is as follows:

3.1. Material Requirements and Certification:

Material Quality and Strength: Strict mechanical and chemical requirements must be met by propeller material in order to endure operational stresses like cyclic loading and avoid failure. Therefore, compliance with classification society certification and detailed testing reports is required to verify that the used material can endure decades of use without degrading performance.

Long-Term Fatigue Resistance: When comparing the material's fatigue strength to acting dynamic stresses, minimum safety factors must be used. These safety factors reflect the risk and criticality related to the specified load conditions, as well as the expected prediction quality of acting loads, corresponding stresses, and fatigue strength of material. As propellers face constant stress from repeated motion, rigorous fatigue testing is important. Class guideline DNV-CG-0039 offers guidance for fatigue testing. This ensures that the material will not crack or fail under high-cycle loading conditions.

Corrosion Protection: Because the material will be exposed to seawater, it should have built-in corrosion resistance or protective treatments (such as heat treatments DNV-RU-SHIP Pt.2 Ch.2 section 8.4.4) to prevent rust and structural damage and prolong the propeller's life even under challenging maritime conditions. Conversely, a hub cap that is strong enough to adequately shield the shaft from water intrusion must be installed.

(DNV-RU-SHIP Pt.2 Ch.2, DNV-RU-SHIP Pt.4 Ch.5 outlines these requirements in detail)

3.2. Typical Alloys and Materials Used

Nickel-Aluminum Bronze (NAB):

- **Usage:** It's by far the most common material for cast propellers.
- **Properties:** NAB alloys combine high strength and excellent corrosion resistance, making them ideal for the cyclic loads and marine environment.

- **Considerations:** Its chemical composition is highly controlled (typically high in copper with additions of aluminum, nickel, and iron), which optimizes mechanical properties that increase the resistance towards cavitation and erosion.

Stainless Steel Alloys:

- **Usage:** Although it's less common than copper-based alloys, stainless steels may be employed in applications demanding higher strength or where design constraints require alternative material properties.

- **Properties:** They provide excellent strength and corrosion resistance; however, their higher density and manufacturing cost mean they are typically reserved for specialized or high-performance designs.

Other Specialized Alloys:

- In some cases, additional copper alloys or even ductile cast irons might be considered, depending on the vessel parameters and operational conditions.

- According to the classification society, for usage of any non-standard material should be supported by comprehensive testing and documentation to ensure its suitability.

3.3. Determining the required blade thickness:

When determining the required blade thickness for a solid propeller, the classification society guidelines lay out a structured approach that balances the hydrodynamic loads with the material's strength. The detailed steps involved in thickness determination are as follows.

3.3.1. Load Analysis and Stress Calculation:

The process starts by calculating the bending moments and stresses acting along the blade due to the hydrodynamic forces. Designers need to assess both high-cycle (fatigue) and low-cycle (peak) stresses. In many cases, special attention is given to the mid-section of the blade (typically around 60% of the blade radius) where the bending moment reaches a critical value.

3.3.2. Correction Factors and Effective Section Modulus:

To account for factors such as the fluctuating load, blade geometry, and thickness effects, several correction factors are applied.

Thickness Correction Factor: It accounts for adjusting the bending stress calculation based on the actual thickness of the blade. This factor helps bridge the gap between idealized calculations and the practical behavior of the blade.

Load Correction Factor: It incorporates the effects of fluctuating loads, which ensure that variations in operating conditions are taken into account.

Skew Correction Factor: It compensates for the blade's inclined geometry, which affects how stresses are distributed across its section.

Effective Section Modulus Coefficient: This further refines calculation of bending resistance, tailoring it to the specific geometry and material properties of the blade.

These factors adjust the basic bending moment calculations to reflect real operating conditions. The outcome of these calculations is the "**effective section modulus**" needed to ensure the blade can safely withstand the loads. The blade's cross-section (and thus its thickness) is then designed so that its actual section modulus meets or exceeds this required value.

3.3.3.   Simplified and Detailed Methods:

For blades operating under standard conditions, a simplified method is sometimes used. This involves setting a minimum profile thickness at a reference section, which is often at 60 or 90% of the radius. The method gives only a simplified idea about thickness and these two points only. Finite Element Analysis (FEA), a more thorough method, can be used to refine the estimations and capture local effects such as stress concentrations at the blade tip or between the reference section and nearby fillets for more intricate details and creative design.

This comprehensive approach is outlined in the DNV guidelines for propeller calculations, where the interplay between bending moment calculations, effective section modulus, and various correction factors is critical for determining the optimal blade thickness.

(For further information, refer to sections in DNV-CG-0039 "Calculation of Marine Propellers": 3.2, 3.3, 3.6, 3.7, 3.8, and 8.)

4. FINITE ELEMENT STRUCTURE SIMULATION:

The blade structure must undergo a Finite Element Analysis under various loadings and boundary conditions specified in accordance with the propeller's application and operating conditions in order to perform a thorough stress analysis, which will lead to the decision on the necessary blade thickness at each section of the propeller blade. A thorough 3D model is first made using the information from hydrodynamic analysis, which is derived from the forces operating on the propeller and in accordance with the necessary power and speed, before beginning FEM analysis. The 3D model of the blade profile is shown in Figure 3.
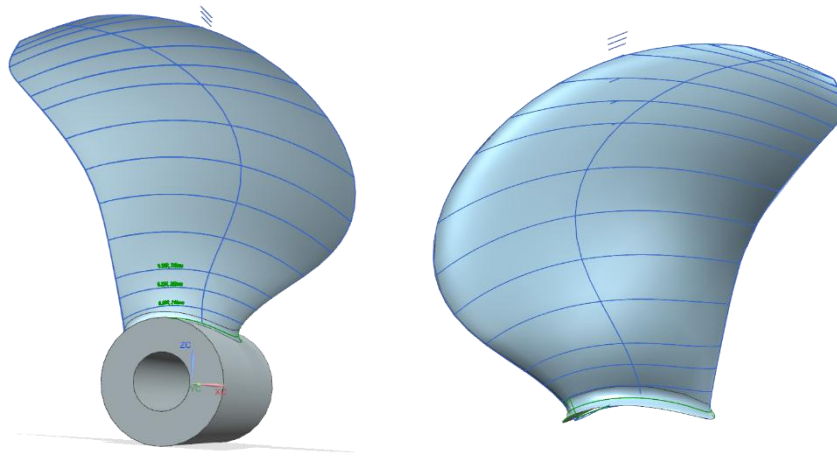
Figure 3 Blade profile with section distribution

A detailed mesh is created on both sides of the blade surfaces once the model is complete and the blade profile is transferred into Ansys Workbench. For initial analysis, a quadratic mesh is used as it works better for curved surfaces because it bends and fits the shape more naturally than a basic mesh. Instead of using straight edges, it has midpoints that help capture curves more smoothly. This means one can get more accurate results without needing a super fine mesh, making simulations more reliable and efficient for things like stress analysis or fluid flow.

For the initial analysis, a uniform pressure is applied to the blade profile, which differs on the suction and pressure sides. Regarding the boundary conditions, the root of the blade is fixed to the propeller hub, while all other sides of the blade are free. The pressure and boundary conditions are illustrated in Figure 4. After that, Von Mises stress and deformation are calculated throughout the blade, and the stress results are shown in Figure 5.
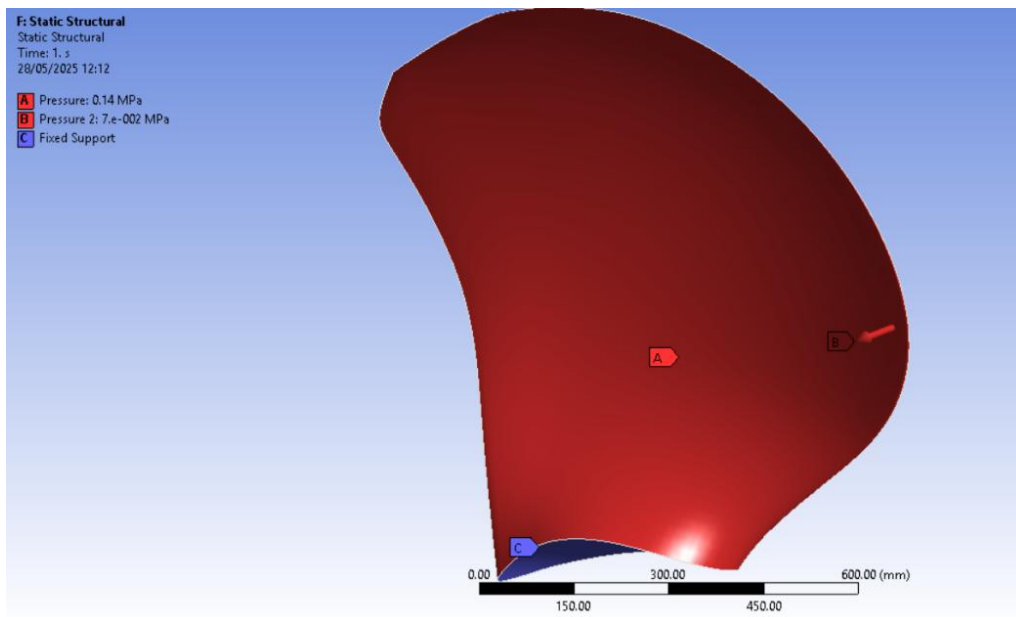
Figure 4 Boundary Condition on Propeller blade
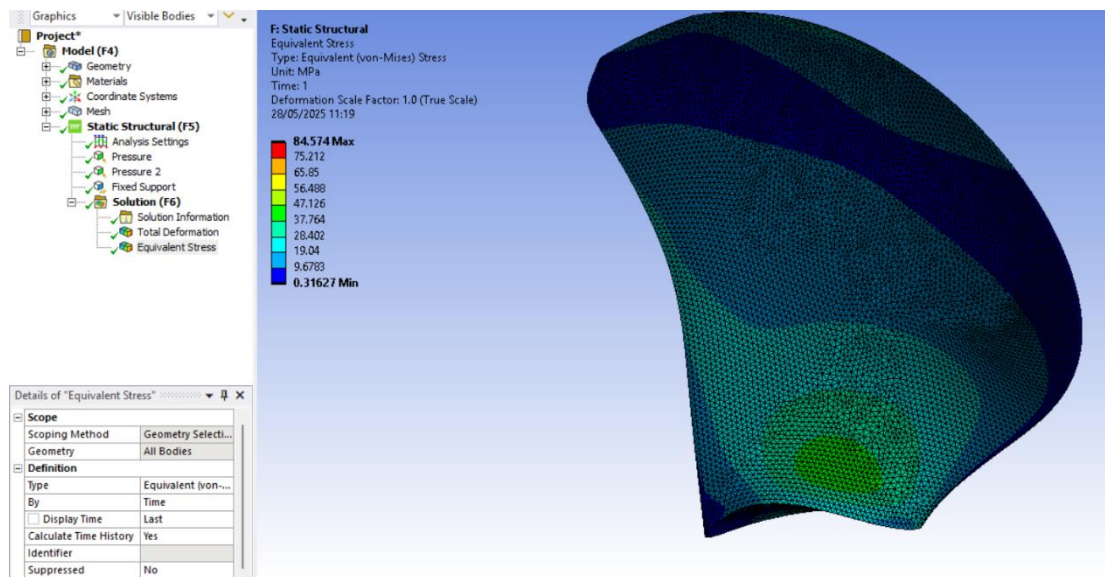
Figure 5 Stress distribution on the propeller blade

As Figure 5 shows, the stress amplitudes on the blade profile, which indicate mean and higher stress, are identified and checked if the stress is within the acceptable limit. As the profile is fixed at the bottom, there are some stress concentration areas (singularity points).

These singularities or High stress concentrations observed at the blade root in the FEM results are attributed to the idealized fixed boundary condition applied at the root. Numerical singularities result from the geometric and stiffness discontinuities that this produces. In practice, such severe localised stresses are avoided by connecting the blade to the hub via a

mechanical joint or gradual transition that more evenly distributes loads. Therefore, stress values very close to the fixed boundary are not physically meaningful and are excluded from the critical stress evaluation. The singularity points are shown in Figure 6.
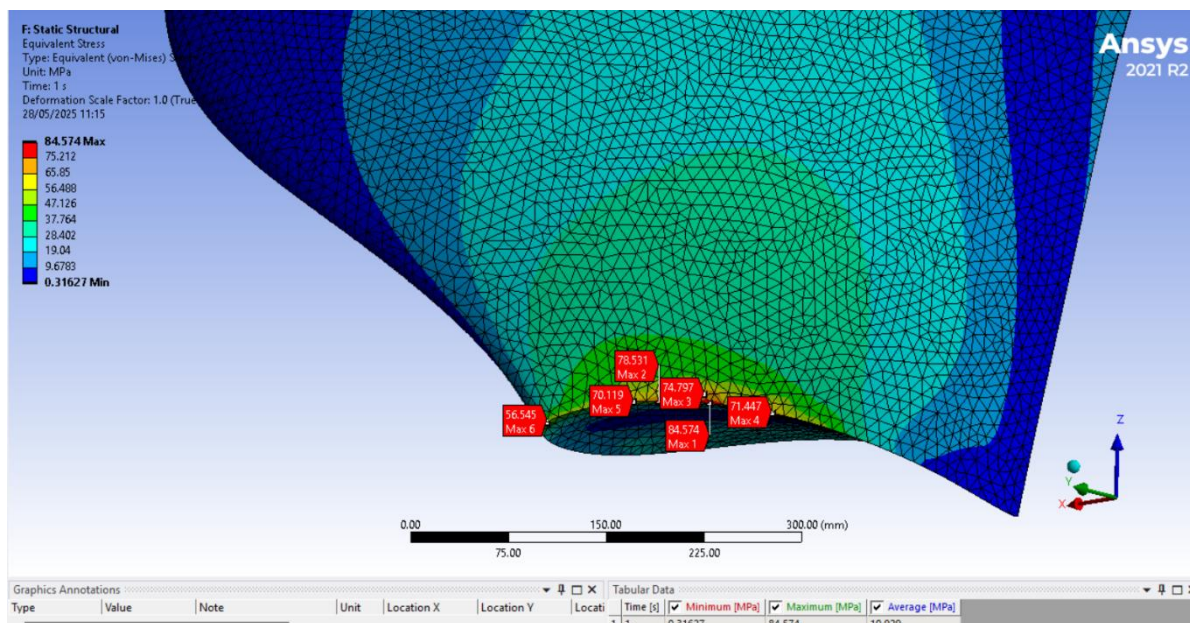
Figure 6 Singularity points at the blade root.

The maximum stress limit for this propeller is 80 MPa, which is achieved when singularities are ignored. As the average stress on the propeller profile is just 10.929 MPa, with the maximum stress area is near radius 0.2, with a maximum value of value of about 44 MPa.

4.1. Fatigue Test Required for Propeller (According to DNV)

Fatigue testing is critical for cast propellers used in maritime applications because of the cyclic loads caused by variable hydrodynamic forces during operation. High-cycle fatigue (HCF) evaluation is a typical criterion for these components because they are subjected to millions of load cycles over their service life. In order to determine whether stresses are within safe bounds and whether a geometric adjustment is necessary to alter the thickness in specific places, this method offers an appropriate stress distribution on both sides of the blade. To guarantee durability and dependability, fatigue life is normally evaluated over a minimum of 10^8 cycles in compliance with standard classification guidelines, such as those offered by DNV.

This page is left blank intensionally.

Chapter # 2

Manufacturing, Material, and Design

1. ADDITIVE MANUFACTURING

Additive manufacturing is a process in which material is added to form a component. It's mainly associated with the 3D printing process in which a component is built up layer by layer from digital designs. The process joins the material in all three dimensions and produces a near-net shape, which means that it produces the part that is very close to the final shape but requires some finishing by milling. However, unlike traditional subtractive manufacturing, which removes material from a solid block, additive manufacturing (AM) adds material only where needed, reducing waste and enabling complex geometries that would otherwise be impossible to create with traditional manufacturing processes.

The process involves creating a 3D computer-aided design (CAD) file, which is then converted into machine instructions (G-codes) using the slicing process. In which different parameters and parts of printing are defined depending on the type of printing technology and selected material.

There are mainly two types of 3D printing technologies used in metal 3D printing at commercial scale. The first one is **Fused Deposition Modeling (FDM)**, also known as **Direct Energy Deposition (DED).** It involves use of a material in the form of a continuous wire or filament, which is melted using a laser beam or arc and deposited layer by layer to build the final component. The final components undergo additional post-processing to achieve the final finish. This process is widely used for its affordability and high deposition rate.

Figure 7 Fused Filament Fabrication (left), Selective Laser Sintering(right) (source:unconfirmed)

Selective Laser Sintering (SLS) is an additive manufacturing process that uses a high-powered laser to fuse powdered material together, layer by layer, to create a solid component. The laser selectively sinters the material based on a digital design, allowing for the production of complex and durable parts without the need for support structures. The main disadvantage of this technology is that the cost of powdered material is very high compared to other manufacturing methods. Therefore, their usage is limited to highly complex or unique components.

2. WAAM METHOD:

For the process of propeller manufacturing, WAAM (Wire Arc Additive Manufacturing) is used, which is a type of Fused Deposition Modeling. As it allows rapid production while being cost-effective. The WAAM process involves feeding a metallic wire through an electric arc, which melts and deposits on the base surface. In this way, the workpiece can be built layer-wise or even subpart by subpart. This method is particularly useful for creating unique and complex metal components as it reduces material and energy usage, which results in lower costs compared to traditional subtractive manufacturing techniques. WAAM is combined with the CNC milling to remove the excess material after printing and create a smoother surface. Both printing and milling processes work simultaneously for complex structures, such as propeller blades, to remove excess material from both inside and outside in the case of a hollow propeller.

Figure 8 Hybrid Manufacturing (WAAM combined with the Milling process) (source: unconfirmed)

The torch is attached to a CNC system or robotic arm that moves following calculated G-codes, which allow the machine to move according to the model shape and control deposition rate. The wire thickness, feeding rate, and welding torch travelling speed are all affect the thickness of the weld.

There are two main types of arc modification used in this WAAM. First is Pulse Multi Control (PMC), which is a welding technique used for making metal deposition more stable and controllable. It carefully managing the pulse of the welding current, PMC helps to reduce spatter, control heat input with deeper weld penetration, and improve the overall quality of each layer, which is important while using a base part that is at colder temperature (otherwise preheating of base part is required) and of lower strength than the printing material, therefore, PMC ensures the proper bonding of the base and printing material that ensure a smoother material deposit, which is important while printing large or complex components.

Second is Cold Metal Transfer (CMT) focuses on reducing heat during welding by quickly pulling the wire back after the metal droplet forms, leading to lower heat input and minimal distortion, which is important in additive manufacturing as the layers need to be cooled down quickly. Therefore, for the main printing process, CMT is used, followed by a few layers with PMC. The CMT is also useful when working with thin materials or metals that are sensitive to heat, as it helps maintain accuracy and prevents warping while still achieving strong welds.

Combining both techniques allows for high material efficiency and the ability to create near-net-shape components, reducing the need for extensive machining afterwards. The WAAM process is shown in Figure 9.
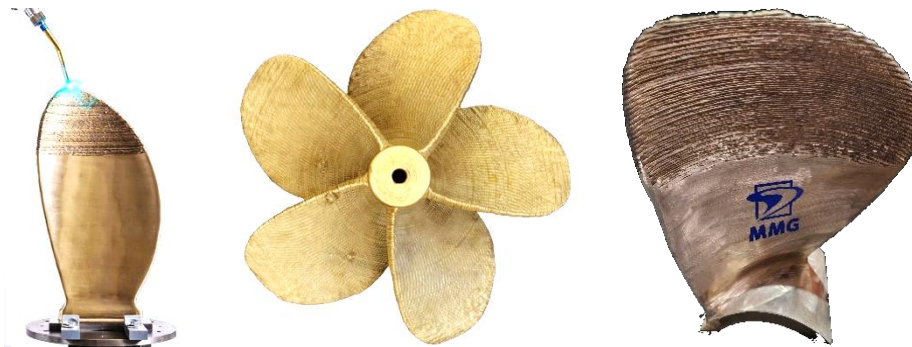
Figure 9 Propeller manufacture by WAAM Process

2.1. Current development status:

Nowadays, WAAM technology is used for a wide range of applications, from manufacturing automotive components to producing parts for aerospace and maritime industries. Large, intricate, and highly-strengthened metal components can now be produced more quickly and with less material waste than with traditional production methods.

In the field of propeller manufacturing, WAAM offers significant advantages by enabling the fabrication of customized and optimized designs with improved efficiency. High-performance alloys for marine applications, like nickel-based alloys, aluminum bronze, and stainless steel, can be used thanks to this WAAM.

The process also enables cost-effective repairs and adjustments to existing propellers, expanding their operating lifespan while limiting downtime.

3. MATERIAL SELECTION FOR WAAM:

Choosing the appropriate material for Wire Arc Additive Manufacturing (WAAM) is an important step that has a direct impact on both the manufacturing process and the long-term performance of the finished component. A number of criteria, including material availability, cost-effectiveness, and durability in challenging environmental circumstances, determine the choice of material.

For marine applications, especially for propellers, the material must offer excellent resistance to corrosion from saltwater. To withstand the cyclic loading encountered during operation, it must also offer strong mechanical qualities such as high strength, sufficient ductility, and good fatigue resistance. Moreover, the WAAM process, particularly when combined with Cold Metal Transfer (CMT), relies on the material's ability to produce consistent high-quality weld beads and have good formability and precise geometries. This material characteristic will help in minimizing the necessity for extensive post-processing and help maintain the integrity of the final part.

Beyond these performance and process requirements, the selected material must comply with established industry standards, specifically those outlined by classification societies. These standards demand that every aspect of material, from its chemical composition to its mechanical properties and as well as its heat treatment history, is well-documented and meets the rigorous criteria for use in marine environments.

3.1. Copper-Based Filler Material:

For material selection for Additive manufacturing using WAAM technology, previous research (Göttsche *et al.*, 2024) this previous study on hybrid manufacturing, three copper-based filler metals were investigated. These are

- CuAl8Ni2Fe2Mn2 (Nickel-Aluminum Bronze)

- CuAl9Ni5Fe3Mn2 (High-Nickel Aluminum Bronze)

- CuMn13Al8Fe3Ni2 (Manganese-Aluminum Bronze)

This study indicates that CuAl9Ni5Fe3Mn2 appears to be the best candidate for the WAAM process because of the following criteria.

3.1.1. Superior Balance of Properties:

Optimized Chemical Composition:

Its composition with approximately 8.5 wt% Al, 3.5 wt% Fe, 0.8 wt% Mn, and 4.5 wt% Ni provides a more balanced mix that supports both high corrosion resistance and good weldability. The higher nickel content (4.5 wt%) improves the resistance to seawater corrosion and enhances arc stability during WAAM processing. (See Table 2 in (Göttsche *et al.*, 2024))

Meeting Classification Requirements:

Its composition aligns well with the classification requirements outlined in DNV documents, ensuring that the finished propeller meets both performance and certification standards. As material compliance is not only critical for ensuring the material's performance in the harsh marine environment, but also for fulfilling the certification criteria outlined in DNV documents

(Refer to DNV guidelines in DNV-CG-0197, Section 1.5, and DNV-RU-SHIP Pt.2 Ch.2)

3.1.2. Process Compatibility and Performance

WAAM Process Efficiency:

- The previous investigations using Cold Metal Transfer (CMT) showed that CuAl9Ni5Fe3Mn2 delivered stable bead geometry and reproducible weld quality.

- Such consistency is vital for the hybrid manufacturing process, where the alternating additive and subtractive steps demand predictable material behavior.

   (Experimental findings are detailed in (Göttsche *et al.*, 2024))

Machinability and Post-Processing:

- The alloy's mechanical characteristics not only support high cyclic fatigue resistance, which is critical for propeller applications, but also allow for efficient milling of both external and internal surfaces of the hollow propeller structure.

3.2. Steel-Based Filler Material

Steel-based alloys are a good candidate for the WAAM process as they are cheaper and abundant compared to Aluminum-Bronze alloys. The alloy used in testing is stainless steel (316L). While this material has relatively lower yield and tensile strength values compared to Aluminum-Bronze CuAl9Ni5Fe3Mn2, it has better elongation. The details are shown in Table 1.

Table 1: Results of static Tensile testing (Göttsche et al., 2024)

Welding Process and Sample Direction	Yield Strength [N/mm2]		Tensile strength [N/mm2]		Elongation [%]	
	Steel	Alu-BZ	Steel	Alu-BZ	Steel	Alu-BZ
CMT horizontal	301	393	584	707	34.0	28.3
CMT vertical	310	384	588	678	36.0	19.8
PMC horizontal	291	402	590	694	34.4	25.2
PMC vertical	292	403	592	684	37.0	19.7
PMC transitional Area	300	332	591	637	36.4	14.1

3.3. Compliance with Classification Rules and Certification Guidelines

DNV-CG-0197 Guidelines: These guidelines (Section 3) establish the framework for qualifying additively manufactured materials. They require that the feedstock and the finished component be documented for chemical composition, mechanical properties, and process controls.

DNV-RU-SHIP Pt.2 Ch.2 (Materials and Welding): This document sets forth the chemical composition and mechanical property requirements. For example, sections that deal with chemical composition (e.g., Sections 2.6 and 2.10) ensure that the selected copper alloys have the proper alloying elements and heat-treatment conditions to meet marine service standards.

DNV-RU-SHIP Pt.4 Ch.5 (Propeller Rules): These rules specify that the materials used in propeller construction must be fully traceable and documented concerning their performance characteristics, such as impact resistance and fatigue behavior, etc. The selected copper-based alloy, which has to be processed by WAAM, should be able to meet these propeller-specific requirements.

4. ROBOT WELDING AND PROCEDURE

Robots have been used in the welding process for many years. Their systems operate on the pre-programmed motion sequences generated by CAM software based on CAD model and orientation of printing, which reduces human error and ensures consistent weld quality throughout the whole part. These systems are compulsory for WAAM, as these robotic arms can continuously deposit material layer-by-layer with uniform flow and heat input. With five to six degrees of freedom, these robots can typically follow complex patterns without the need for a support structure like polymer 3D printers. In addition to increasing process efficiency, these robotic welding techniques are reducing residual stresses and thermal distortions, two major issues in the production of large, intricate components like propellers. Detail configuration is shown Appendix.

4.1. Robots used in Welding Systems:

4.1.1. *Articulated Robotic Systems:*

Usually known as Robotic arms. These robots are equipped with rotary joints that provide a wide range of motion, which makes them suitable for the complex geometries found in propeller blades.

The robotic arm used in our setup is a Kuka ██████████████████████████ ██ ████████████████████████████

4.1.2. *Positioner Systems:*

These robots act as a base for manufacturing or holding parts. The positioner robot used in our setup is a Kuka ████████████████████████████████████ ██ ████████████████████████████████

4.1.3. *Key Components:*

The main Key Components of a Robotic Welding System that ensure a reliable and stable welding process are as follows

- **Manipulator (Robot Arm):** Controls the welding torch and follows programmed tool paths.
- **Rotatory Base:** Use for turning or rolling the workpiece in 2 axes.
- **Power Source**: Provides the necessary current and voltage for stable arc welding.
- **Wire Feeding System**: Ensures continuous material supply for deposition.
- **Shielding Gas System**: Protects the weld pool from oxidation.
- **Seam Tracking System:** Adjusts the torch position in real-time to maintain weld quality.
- **Safety Enclosures:** Protects operators from arc radiation and high temperatures.

Robotic welding, when integrated with WAAM, allows for highly controlled metal deposition, improving efficiency and quality in propeller manufacturing while reducing the need for extensive post-processing.

(Reference: DNV-CG-0162)

4.2. Welding Procedure:

The system has a base section mounted on the positioner and a welding torch mounted on a robotic arm. Throughout the building process, this setup enables precise control over the robotic movement and material supply rate.

The manufacturing process begins with arc cladding, which involves melting the base material to form a strong metallurgical bond with the deposited layers. In order to maximise fusion between the substrate and the first deposition layer and avoid flaws such as excessive dilution or lack of fusion, Pulse Multi Control (PMC) is utilised for the initial layer. The Cold Metal Transfer (CMT) procedure, which reduces heat input, residual strains, and distortion while guaranteeing a stable and uniform deposition, is then used to build up the next layers.

Throughout the process, Gas Metal Arc Welding (GMAW) is deployed as the heat source with predefined parameters: voltage, current, and wire feed speed for the selected defined alloy. A shielding gas environment, primarily argon, is maintained to prevent oxidation and contamination of the molten pool. As the deposition occurs in a layer-by-layer manner, the toolpath is pre-programmed and optimized for minimal thermal distortion and uniform mechanical properties.

To ensure high quality build, real-time monitoring systems are employed to adjust parameters dynamically, compensating for any deviations during deposition. The deposited structure undergoes periodic interpass temperature control, which prevents excessive heat accumulation while maintaining the material integrity. During the building phase the deposition process is pause time to time to allow the surface finishing of part via milling process, this hybrid process allow the machining of complex parts with curvature and inner structure, Once the component is fully built, post-processing steps such as heat treatment (if required), and non-destructive testing (NDT) are carried out to check dimensional accuracy and verify structural integrity.

This orderly methodology allows the WAAM process to produce propellers that satisfy tough mechanical properties and dimensional accuracy while optimizing material efficiency and reducing production time in contrast to conventional manufacturing techniques.

4.3.Manufacturing Constraints:

There are many constraints that have to be considered while moving from the design stage to manufacturing. Most of these constraints are due to limited technical capability, while a few are due to Material limitations.

The following manufacturing parameters have to be taken into account.
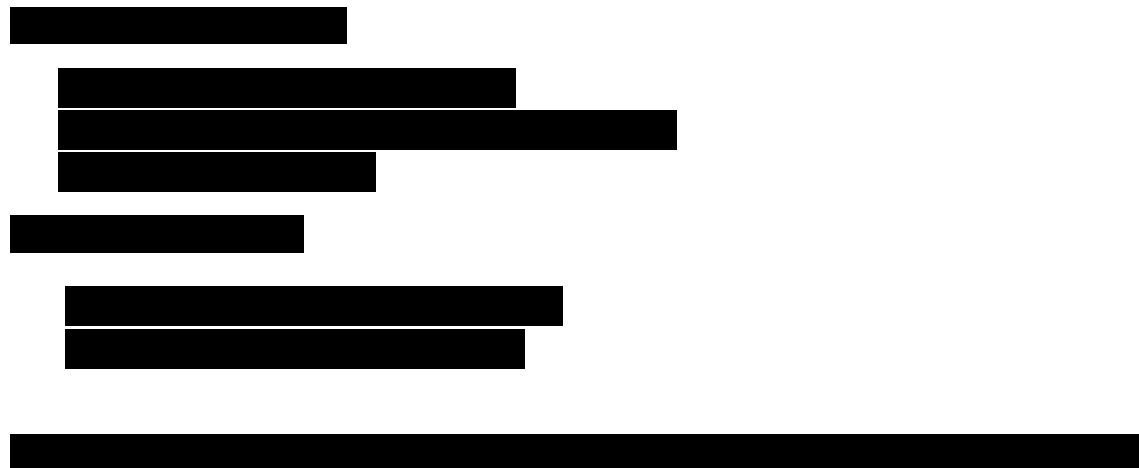
5. PROPELLER GEOMETRY:

The Propeller geometry used in this project consists of a Right-handed propeller with five blades and a radius of 1 meter. The detailed specifications are mentioned in the appendix (later). The geometry can be seen in Figure 10.
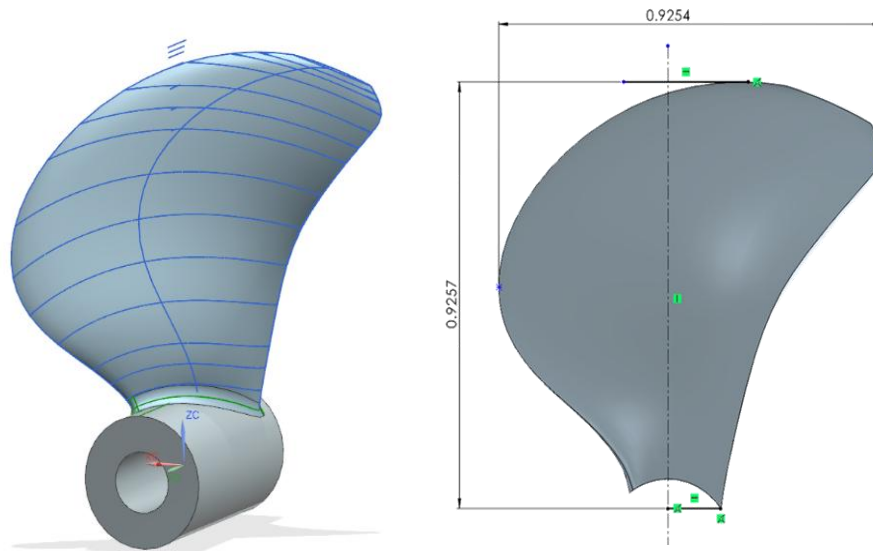
Figure 10 Propeller blade with hub

This propeller geometry is manufacturable with currently available WAAM equipment. A hollow model of the propeller geometry is also created with a shell thickness of 9mm. As shown in Figure 11, the whole geometry is not hollow; only about 80 % of geometry is hollow because of small thickness at the blade tip and edges.
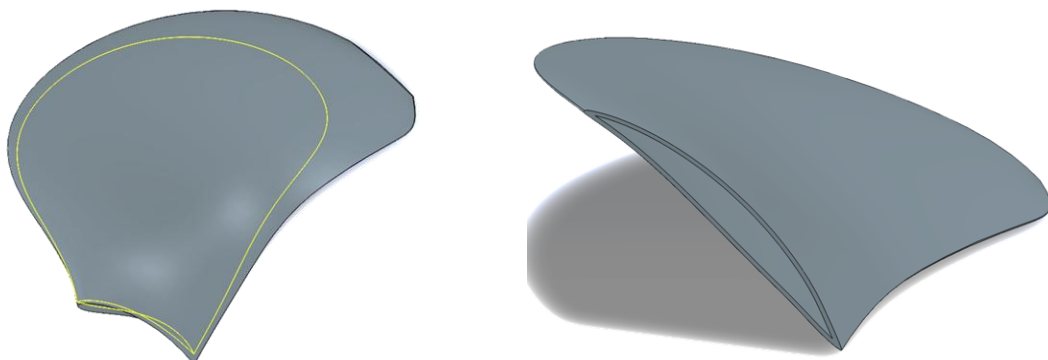
Figure 11 Propeller with shell structure at 9mm thickness

5.1. Hollow Structures:

Additive manufacturing process allows for to manufacture of propellers with a hollow profile or with an internal structure instead of using a typical solid profile. This method allows for the reduction of manufacturing time, material consumption, and total cost of small propellers and components. But first, a thorough investigation is needed to analyse these hollow structures and internal structures in detail, in order to determine whether these structures fulfil the required design criteria and what parameters are required to make these structures feasible for different loading.

5.1.1. *Previous method of Stress Analysis and suggesting internal structures:*

As the propeller consists of multiple blades and a hub, where all the main loadings are applied on the blade surface due to fluctuating hydrodynamic pressure, and this pressure is exerted on the blade depending on the surface area of the blade. The main stresses that are acting on the blade are bending stresses, which lead to deformation of the blade. A blade with a larger blade area has lower stresses under the condition of the same propeller thrust/loading; therefore cross-section with a higher area moment of inertia is required to design the internal structure.

A simplified method is employed in the previous analysis to examine the relationship between area and moment of inertia. This method involves considering an ellipsoidal profile with a single point load acting perpendicular to the cross-section, as shown in Figure 12. The point load is acting along the Y-axis, which will generate bending and moment in the Z-axis. There are four different geometries considered for analysis.

- Solid
- Hollow with 8 mm wall thickness
- Hollow with 5 mm wall thickness
- Hollow with 5 mm wall thickness and a web.

A non-dimensional parameter 'K' is defined, which is a ratio of the area of cross-section to the moment area of inertia; this parameter will show the efficiency of different cross-sections.

$$K = \frac{A^2}{I_z} \tag{6}$$

The structure with a higher I_z value and a smaller area is the best candidate, as it means that the area at which pressure is acting is smaller than the area moment of inertia of the structure, which

means a highly efficient structure. Which in this case is hollow profile with the smallest wall thickness of 5mm.

On the other hand, as the structure becomes hollow, it is more prone to bending at relatively lower loading. So, a compromise has to be made between a highly efficient structure and buckling strength. The best way of optimizing this structure is to create a support structure between the two faces of the hollow blade profile. Therefore, for initial studies, two types of structure were considered for further analysis.

Figure 12 Simplified section with single and double support

These structures were then compared with different support thicknesses and support joints with the main structure, and all the studies were based on these two simplified geometries.

Now, a proper stress analysis of a realistic blade profile, a modern mathematical approach is required, which is discussed in the next chapter.

Chapter # 3

Internal Design and Structure Optimization

1. INTERNAL STRUCTURES

The typical manufacturing method involves the production of Components in either solid or hollow structure, as these geometries are easy to manufacture using traditional manufacturing techniques, but this approach always involves some compromises, for the components that are exposed to high stresses are generally made solid, which leads to wastage of material and increases the mass of the final component. On the other hand, for less intensive applications, manufacturers go with hollow geometry, which also has its limitations and disadvantages. The modern manufacturing technique, like Additive Manufacturing (AM), acts as a bridge between these two traditional approaches by allowing to creation of internal structure inside a geometry, which helps distribute the load throughout the geometry it being 100% solid. Along with the lower weight, these internal structures help to save cost as a lot of material can be saved through this method.

Many types of internal structures can be created inside a geometry based on the required application. So, for creating internal structure inside the propeller geometry, three different approaches are considered for the detailed study and investigation. which are as follows.

1) Structure Optimization (Topology)
2) Pattern structures
3) Lattice Structure (Bio-inspire)

All these types of internal structure are structures that can be created inside a part or geometry, which help carry or distribute the loads throughout the whole geometry. These techniques can be applied to propellers made with WAAM engineering. Although the propeller blade's interior structure will change as it rises in height, a tiny portion of the blade is removed for the various analyses. A visualization of different types of internal structures inside a propeller blade profile at the 0.5 radius is shown in Figure 13. The first is a simple hollow section of a blade, the second geometry is an example of a topologically optimized structure, the third geometry is an example of a pattern structure with a honeycomb internal structure, fourth geometry is an example of bio bio-inspired lattice structure (Voronoi-Based).
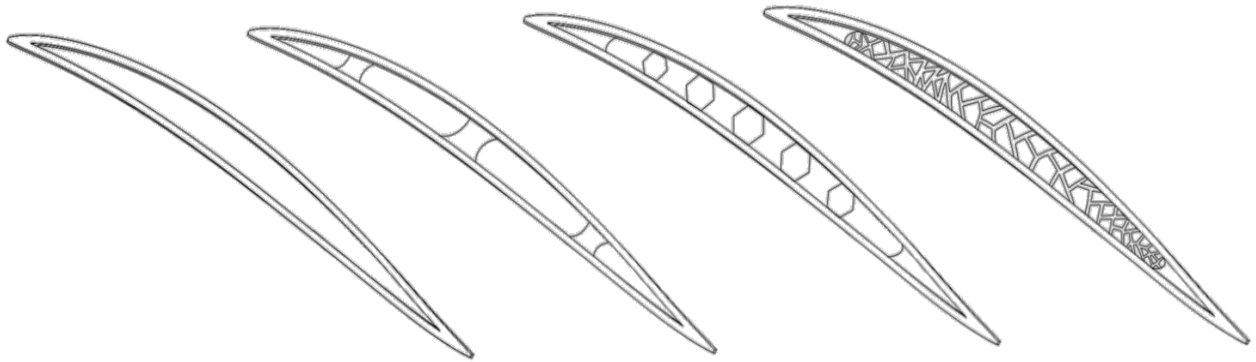
Figure 13 Propeller Blade with different types of Internal structure.

The 1st geometry of Figure 13 represents a hollow blade section, the 2nd geometry is an example of a topologically optimized structure, the 3rd geometry shows the blade section with a patterned internal structure, and the 4th geometry represents a bio-inspired lattice structure.

2. TOPOLOGY OPTIMIZATION:

It's is a mathematical and computational design technique used to find the best material layout within a given design space, subject to loads, boundary conditions, and constraints. Topology optimisation begins with a blank or fully filled domain and mathematically shapes it by eliminating material that does not significantly contribute to structural performance, in contrast to traditional design approaches that frequently start with an established shape or form. In order to meet stress and manufacturability requirements, the goal is frequently to minimise weight, increase stiffness, or enhance natural frequency.

2.1.Mathematical Parameters:

2.1.1. Domain and Design Variables:

The structure occupies a domain Ω that is discretized into finite elements. Each element has an associated design variable x_i.

- $\mu_i/x_i = 1$ material is present
- $\mu_i/x_i = 0$ material is removed (void)
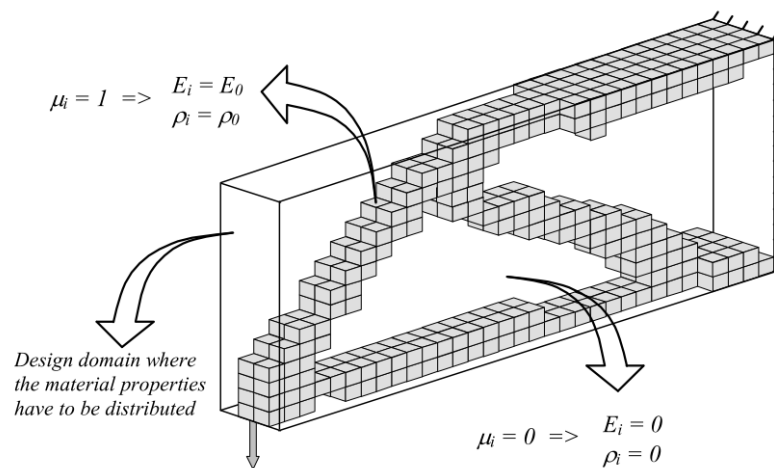
Figure 14 Design Domain (source: Uliege Lectures)

2.1.2. Objective function

Minimize the compliance, which means to maximize stiffness (in this case).

$$C(x_i) = F^T U(x_i) \tag{7}$$

- F is a global load vector
- $U(x_i)$ is displacement vector (depends on the material).

2.1.3. Finite Element Equation:

These displacement vectors are obtained by solving global equilibrium equation.

$$K(x)u = F \qquad (8)$$

Here, K(x) is the global stiffness matrix built from the element stiffnesses scaled by (x_i^p) where p is a penalization factor.

2.1.4. Penalty Function:

It forces design variables towards 0 (void) or 1 (solid), avoiding gray or porous regions.

The stiffness of an element can be interpolated as:

$$K_i(x) = x_i^p K_0 \qquad (9)$$

- x_i = density of element (i).
- p = penalization function (commonly 3).
- K_0= Stiffness of solid material.

Higher (P) $\implies$ Stronger Penlty $\implies$ Sharper Boundaries

$p = 1 \qquad\qquad p = 2 \qquad\qquad p = 3$
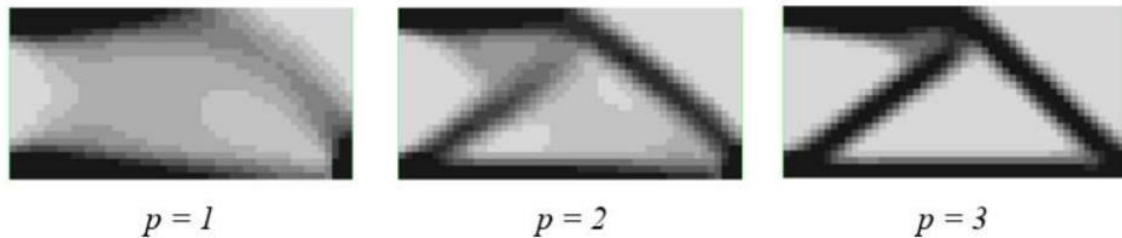
Figure 15 Penalty Function (source:Uliege Lectures)

2.1.5. Volume Constraints:

Volume constraint limits the maximum percentage of the total design space that can be filled with material. It forces the algorithm to prioritize load paths and remove non-essential material.

$$\sum_i^n x_i v_i \leq V^* \qquad (10)$$

- v_i= volume of an element.
- V^*= maximum allowed volume.

2.1.6. Mass Constrain:

Instead of limiting the volume, one can limit the total mass of design. This is important when.

1. The material is non-uniform (has different densities).
2. Gravitational or any inertial loads (like acceleration) are involved.

$$M(x) = \sum_i^n x_i \rho_i v_i \tag{11}$$

- ρ_i = density of material in element i.

In the majority of topology optimization problems, mass and volume constraints are practically interchangeable, provided that ρ_i remains constant. However, when optimizing rotating or weight reduction parts, where inertial mass is important, mass limits are more physically precise. If the design uses uniform material, then both volume and mass constraints yield nearly the same result. If using a multimaterial or varying density, use mass constraint.

2.1.7. *Complete Optimization Problem*

The classic structural topology optimization problem can be formulated as:

$$\min_{x \in [0,1]} C(x_i) = F^T U(x_i) \tag{12}$$

Subject to:

$$\boldsymbol{K(x)U = F} \tag{13}$$

$$\sum_i^n x_i v_i \leq V^* \tag{14}$$

$$x_i \in [0,1] \tag{15}$$

Where:

- x_i is the design variable for element i represents material density (0 = void, 1 = solid).
- C is the compliance (inverse of stiffness), so minimizing C maximizes stiffness.

2.2. Topol Software Parameters:

NX Samcef Topol module is utilized here for topology analysis according to the defined mathematical parameters.

2.2.1. *Filter Radius*

It controls how much the material distribution of one element influences its neighboring elements.

It helps prevent checkerboard patterns and mesh dependencies, which are artificial and physically meaningless oscillations in the results.

- **Small filter radius:** fine features but greater risk of instability.
- **Larger filter radius**: smooth design, but may eliminate small details.
- **Typical Value:** 1.5–3 times the element size.

$$\tilde{\rho}_i = \frac{\sum_{j \in N(i)} w_{ij} p_j}{\sum_{j \in N(i)} w_{ij}}, \quad w_{ij} = \max\big(0, r_{min} - dist(i,j)\big) \tag{16}$$

Where r_{min} is the filter radius, and N_i is the neighborhood of element i.
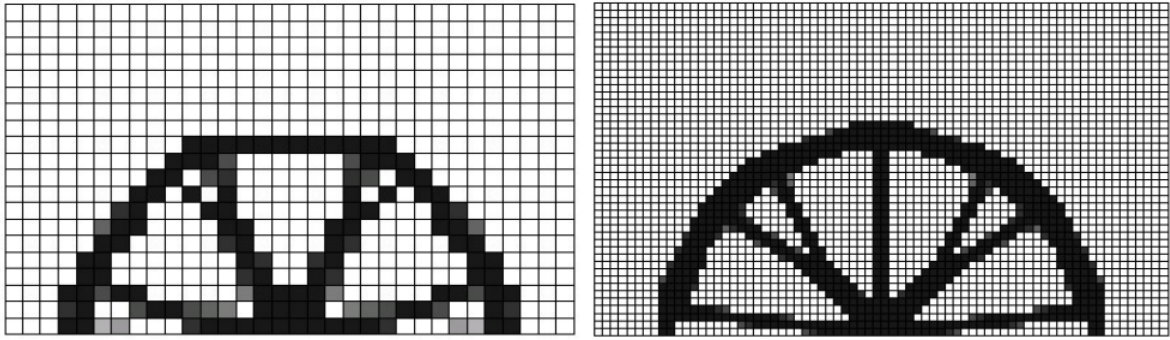
Figure 16 Filter radius example (source:Uliege Lectures)

2.2.2. SIMP Method (Solid Isotropic Material with Penalization):

A popular interpolation scheme is used to relate material density to stiffness.

$$E_i = E_{min} + x_i^p (E_0 - E_{min}) \tag{17}$$

- E_0: Young's modulus of solid material.
- E_{min}: Small value to avoid a singular stiffness matrix.
- P = Penalization factor.

2.3. Different types of Optimizers:

2.3.1. SPOT (Polynomial-based Optimization:

SPOT solves optimization problems using polynomial interpolations of sensitivities. The compliance objective:

$$\min_{x_i} C(x_i) = \mathbf{F}^T \mathbf{U}(x_i) \tag{18}$$

Is minimized using iterative update:

$$x^{(k+1)} = x^{(k)} - \alpha.\frac{\partial C}{\partial x} \tag{19}$$

with filter and projection steps applied after every iteration. Polynomial fitting is used to interpolate gradient trends for convergence acceleration. The main key points are:

- It's a gradient-based technique.
- It can handle volume constraints well.
- It's more efficient for compliance-based problems.

2.3.2. GCM (General Convex Method)

GCM is a dual optimization method. It transforms the constrained optimization problem:

$$\min f(x) \qquad subject\ to\ g_i(x) \leq 0$$

Into a convex subproblem using Taylor approximations:

$$f(x) \approx f(x_k) + \nabla f(x_k)^T (x - x_k) \tag{20}$$

$$g_i(x) \approx g_i(x_k) + \nabla g_i(x_k)^T (x - x_k) \tag{21}$$

and solves the approximate subproblem iteratively. It's more versatile and robust for multi-physics applications (stress, displacement, volume).

The main key points are:

- It can handle complex multiple constraints.
- It's based on convex approximation theory.
- It's more general but slower than SPOT.

2.4. Optimization Parameters for Propeller Blade:

2.4.1. Objective:

Optimize the internal topology of a 3D-printed propeller blade:

- Maintain outer shell thickness
- Reduce internal material
- Maintain mechanical performance close to a solid blade (maximum Stiffness).

2.4.2. Boundary Load Conditions

Apply pressure loads to respective faces.

- Average Pressure side: 0.14 MPa (5.88)
- Average Suction side: 0.07 MPa (2.73)

Apply fixed constraints on the blade root.

2.4.3. Design Space Setup:

- Use CAD to define the full blade, including outer shell
- Separate outer shell geometry to **exclude from optimization.**

2.4.4. Mesh and Geometry

- Mesh the internal volume finely.
- Coarser mesh acceptable in excluded regions.

2.4.5. Output and Interpretation

- Export optimized result.
- Retain voids only inside the blade while outer shape remains untouched.

2.5. Initial Analysis:

At first, the blade file is imported into NX, and a small section of the blade at a radius of **0.2 to 0.3 R** is taken for analysis. As shown in Figure 17.
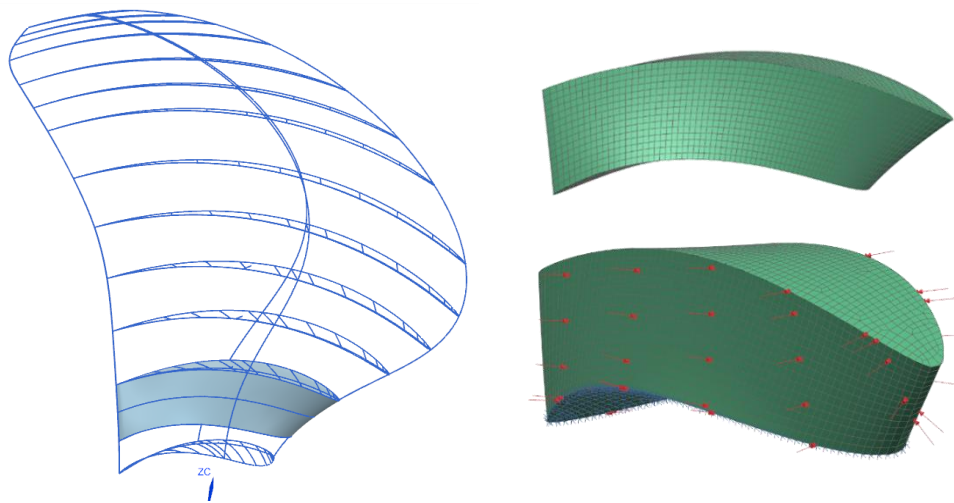
Figure 17 Blade section and FEM analysis

After that, the material is defined, and a hexahedral mesh with an element size of 5mm is created. The final mesh is shown in Figure 17. The material prosperity of aluminum bronze is as follows.

- Density: 7510 kg/m^3
- Young Modulus: 125 GPa
- Poisson ratio: 0.33
- Yield Strength: 323 MPa
- Tensile Strength: 637 MPa

2.5.1. FEM Analysis of Blade section:

The next step is loading the simulation or FEM analysis. The pressure field data is used to implement the loads for analysis. To obtain comparable stress values for the section compared to the entire blade area, the actual pressure field data for the entire blade section were adjusted by a constant factor.

To reduce computational cost while preserving mechanical accuracy, the propeller blade section (from radial position R2 to R3) is used for structural analysis. In order to achieve comparable deformation and stress results between the sectional and full blade models, a localized averaging approach is used, and the applied pressure field on the isolated section is scaled. The section from full blade stress analysis is isolated as shown in Figure 18.

Figure 18 Full blade with section R2-R3 seperated

The scaling factor is determined by subjecting both the full blade model and the section model to the same unscaled pressure field. In contrast to a global averaging approach, the average von Mises stress is extracted only from the R2–R3 region of the full blade, which corresponds to the geometry of the sectional model. This localized comparison ensures consistency in evaluating mechanical response between the two configurations.
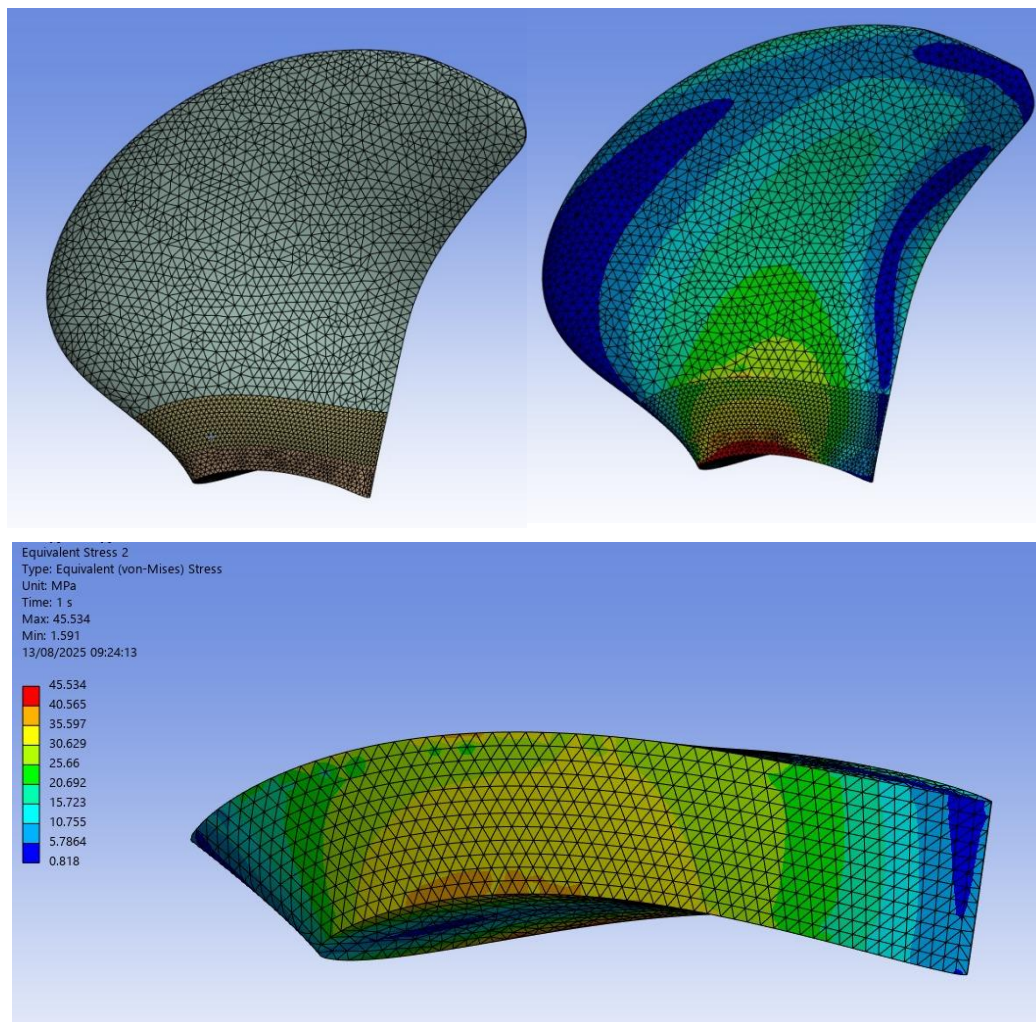
$$Scalling\ Factor = \frac{Average\ stress\ in\ R2 - R3\ section\ of\ full\ blade}{Average\ stress\ in\ isolated\ blade\ section} \tag{22}$$

The actual aerodynamic pressure values on the suction and pressure sides are multiplied by this scaling factor to create an equivalent load field that results in realistic deformation and stress levels in the sectional model. This method improves the fidelity of the simulation by accounting for both local geometry and the actual stress distribution in the corresponding region of the full blade.

This approach provides a more physically representative loading condition and ensures that the sectional model responds in a way that is consistent with the behavior of the full blade, without introducing the inaccuracies associated with global averaging

The detailed values for pressure scaling are given in Table 2 below.

Table 2: Actual and Modified Pressure Values

Component	Values	Scale factor
Average stress in Full-scale	13.516 MPa	43.423
Average stress in Blade Section	0.3113 MPa	
From Actual to scaled pressure values		
0.14 (MPa)	Pressure Side	6.08 (MPa)
0.07 (MPa)	Suction side	3.04 (MPa)

In order to simplify, the boundary condition is predicated on a simplified assumption that takes into account the real blade constraints because the blade section is taken for analysis. As seen in Figure 17, the section's root is regarded as a fixed constraint. On the other hand, the top surface is regarded as free. Following the acquisition of the section deformation and stress analysis results, NX TOPOL receives them for the topology analysis.

2.6. Optimization using NX TOPOL:

The results obtained from the FEM analysis are used as input for the Topology analysis in TOPOL. The main settings for this analysis are obtained after some iterative processes, and the best suitable parameters are found and stated below.

2.6.1. Optimization Settings (NX Samcef Topol):

These parameters are shown in Figure 19.
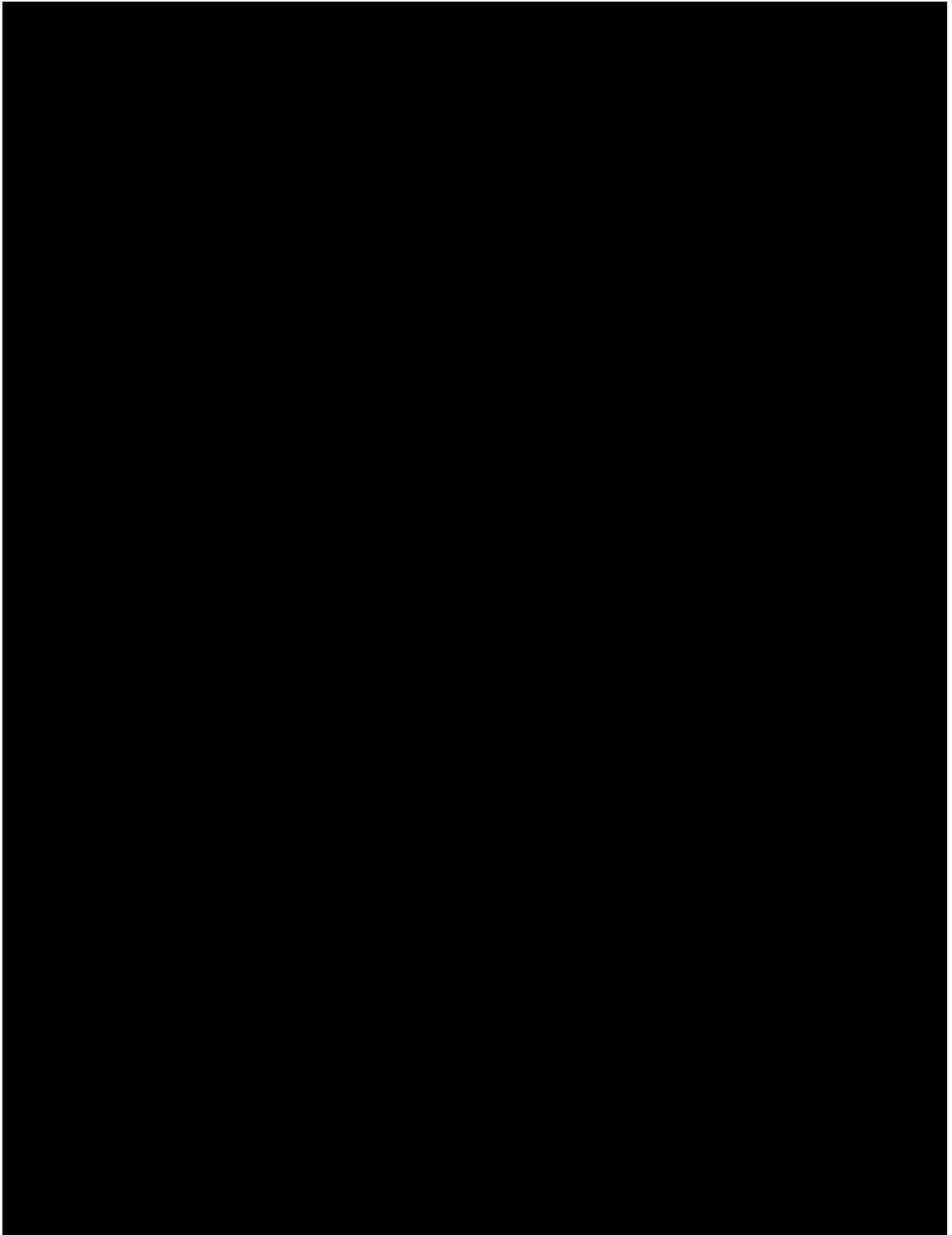
Figure 19 TOPOL Main Parameters

3. TOPOLOGY RESULTS AND ANALYSIS:

After defining the mathematical parameters in side TOPOL. The initial threshold was set at 99.6% the solution reached convergence in 75 iterations. Convergence results are shown in Graph 3.
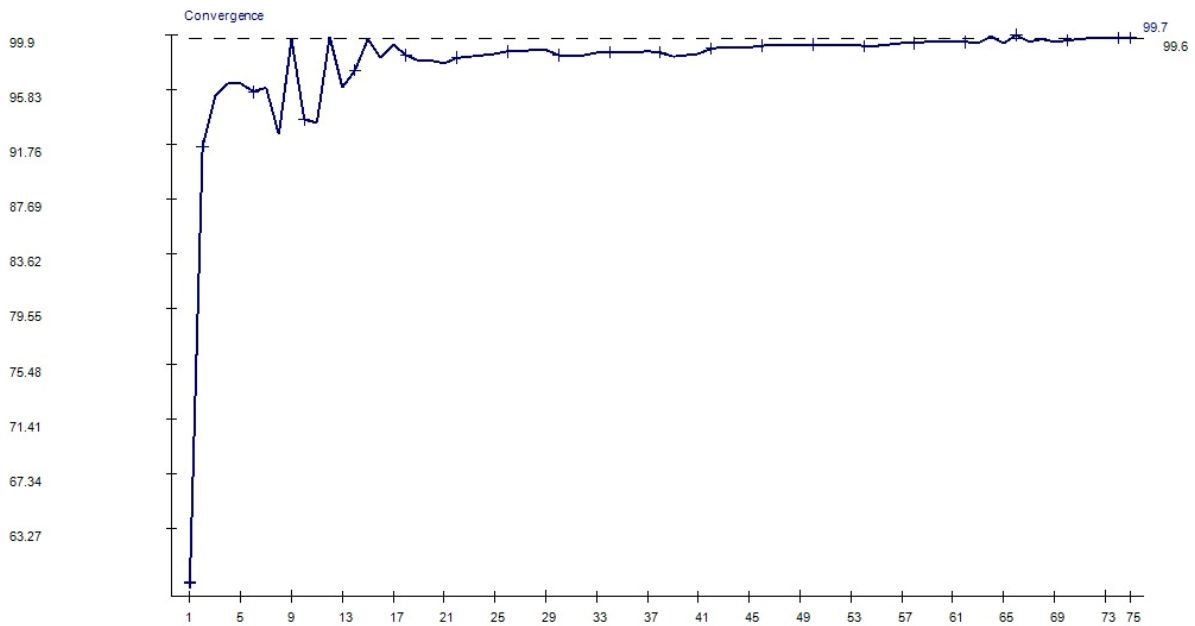
Graph 3 Convergence vs No of Iterations

- Graph 3 shows that the optimization **converged successfully** and efficiently, at 99.7%, which indicates that the optimized result is very close to the mathematical minimum of the objective function (compliance).
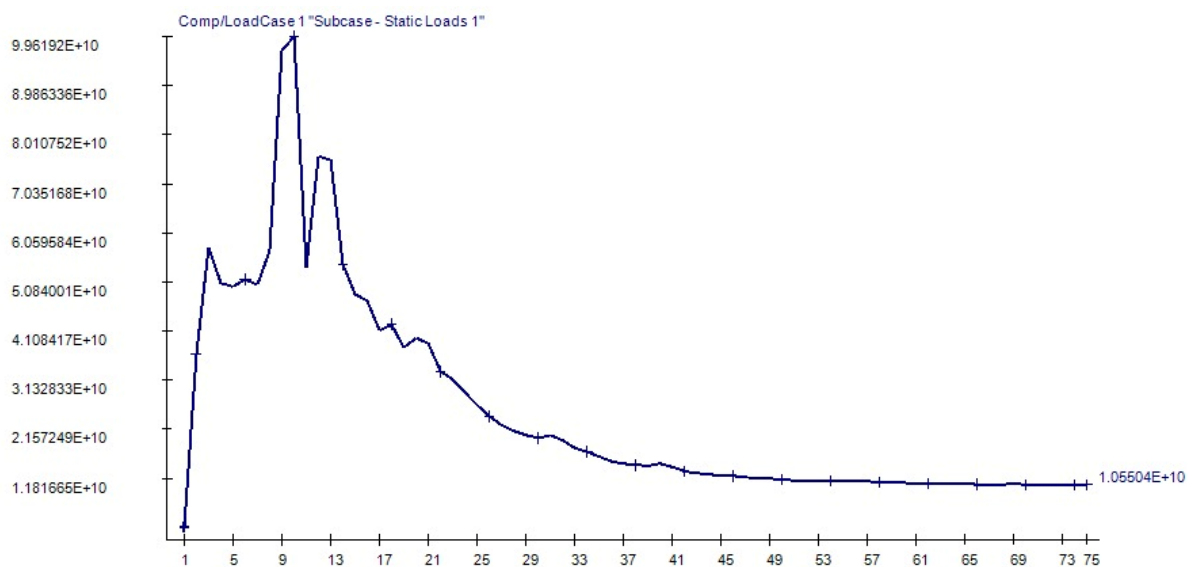
Graph 4 Compliance vs No of Iterations

- Early oscillations in Graph 3 are normal as the optimizer balances material distribution while honoring volume and boundary constraints.

As shown in Graph 4, the graph of Compliance starts high and **decreases sharply in early iterations**, gradually leveling off by iteration ~50 and stabilizing.

- As Compliance is the measure of **flexibility**, which, if lower, is better as it indicates more stiffness. The **rapid drop** in the graph shows that the structure quickly finds a stiffer configuration using less material.
- And the Final compliance ~1.05×10^{10} suggests a **stiff but lightweight** structure, meaning the design efficiently resists deformation under applied loads.
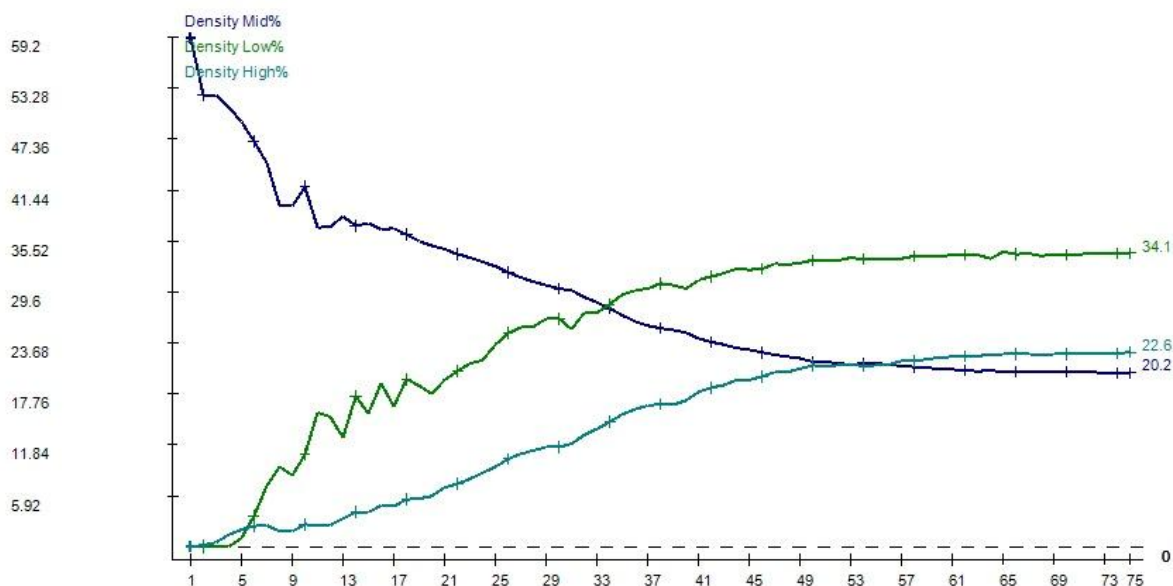
Graph 5 Different Densities vs No of Iterations

The Graph 5 shows the distribution of different densities, which are explained below.

o **High Density %** increases and stabilizes near 22.6%. These areas are critical for structural integrity, bearing significant loads or stresses. The increase and stabilization suggest that the optimization process has identified these regions as essential for maintaining strength.

o **Low Density %** increases and stabilizes near 34.1%. These areas are less critical structurally and may be candidates for material removal, leading to weight reduction without compromising performance. The increase and stabilization imply that the design has effectively identified non-essential regions.

o **Mid Density %** decreases significantly from 59% to about 20.2%. These transitional zones are being reduced, indicating a refinement in the design where material is either being consolidated into high-density regions or removed to create low-density areas, enhancing efficiency.

These density distributions indicate the **clear material separation** (black or white) instead of gray (intermediate), as the optimizer is driving the design towards **distinct solid and void regions**, improving manufacturability. The Mid-density elements are being eliminated over iterations.

3.1. Visual Representation of Structure:

After the solution is converged, the TOPOL module in NX simulation is opened to visualize the results of mathematical optimization. The visual representation of final topological solution is shown in Figure 20.
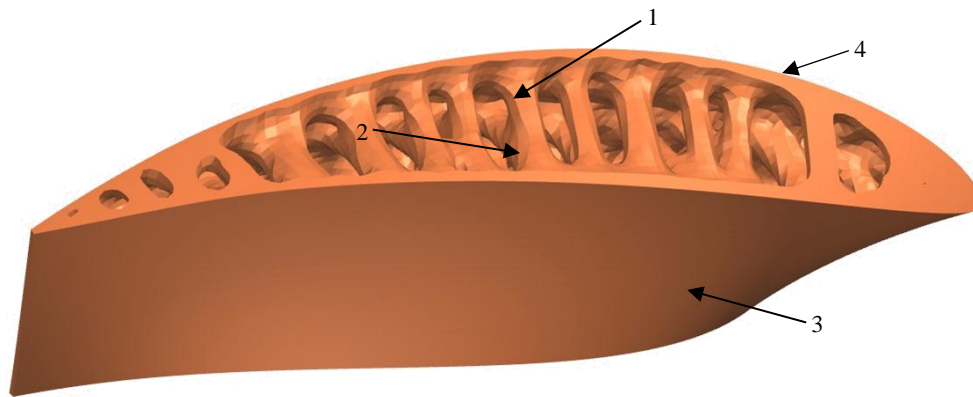
Figure 20 Topology Optimization of blade section

The topologically optimized structure, derived based on the applied pressure distribution across the propeller blade, reveals a well-defined internal branching pattern. Notably, the optimization resulted in a robust single strut-like structure (2) extending from the pressure side (3) of the blade, which corresponds to the region of higher applied load. This outcome is consistent with the boundary condition where the average pressure on this face reaches approximately 0.14 MPa.

In contrast, the suction side (4), which is subjected to a relatively lower average pressure of 0.07 MPa, exhibits a bifurcated, more slender support configuration (1). This dual-branch feature suggests a lower stress demand in that region, allowing the optimization algorithm to remove material more aggressively without compromising structural integrity. The resulting material distribution clearly demonstrates the optimizer's ability to place material efficiently along principal stress paths while maintaining compliance constraints and preserving the outer shell.

3.2. Topology Analysis using NX Topology (black-box):

In addition to the NX Samcef TOPOL module, which is a powerful and mathematically rigorous tool for structural topology optimisation, Siemens NX provides a more user-friendly alternative known as the "Topology Optimisation" module. While on one hand, TOPOL provides fine-grained control over advanced parameters such as filter radius, penalty exponent, optimization algorithm (e.g., GCM or SPOT), and density filtering techniques, the standard Topology Optimization module focuses on ease of use and accessibility. It allows users to define basic optimization objectives and constraints, but does not expose the deeper algorithmic controls available in TOPOL.

The key advantages of the NX Topology Optimization module are its well-developed graphical user interface (GUI), which provides real-time visual feedback and intuitive control over the setup process. This makes it particularly suitable for rapid conceptual design, early-stage development, and industrial applications where speed and simplicity are prioritized over absolute optimization fidelity.
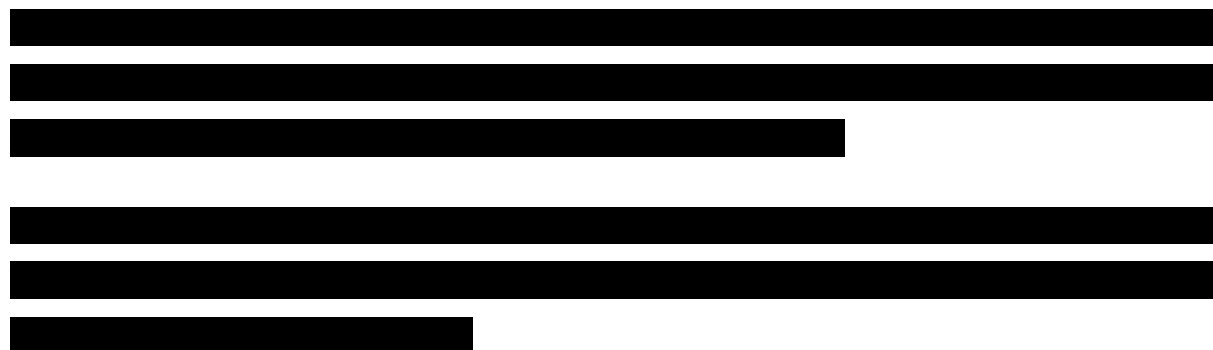
The topology optimization results obtained using the NX Topology Optimizer closely align with those generated through NX Samcef TOPOL. Both methods produced an internal structure that included a thicker, singular support toward the pressure side of the blade section and a narrower, double-branch configuration on the suction side, as shown in Figure 22. This consistency validates the reliability of the NX Topology Optimizer for achieving physically meaningful designs while fulfilling all main constraints.
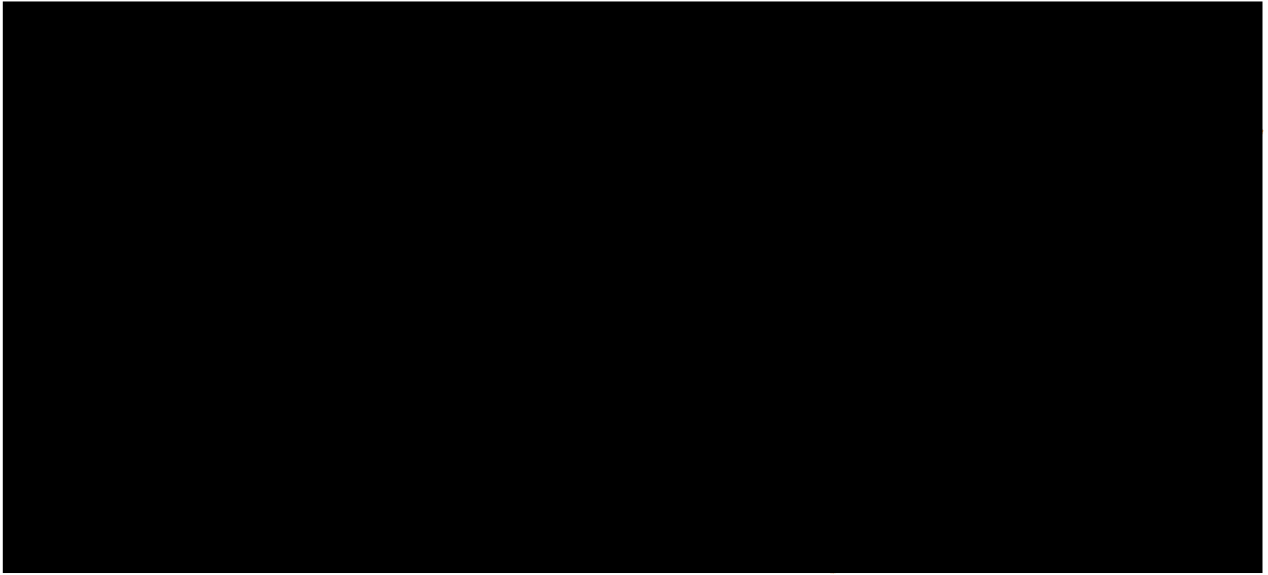
Figure 21 NX Topology Optimizer Parameters

Although the Samcef TOPOL module offers a deeper level of control over the mathematical aspects of the optimization process, such as custom penalty functions, filter settings, and algorithm selection, the newer NX Topology Optimizer has its advantages. It simplifies the setup by focusing on the most essential design inputs, like constraints and objective functions, without requiring extensive knowledge of underlying numerical methods. This makes it particularly useful in industrial settings, allowing for faster decision-making in practical engineering workflows.
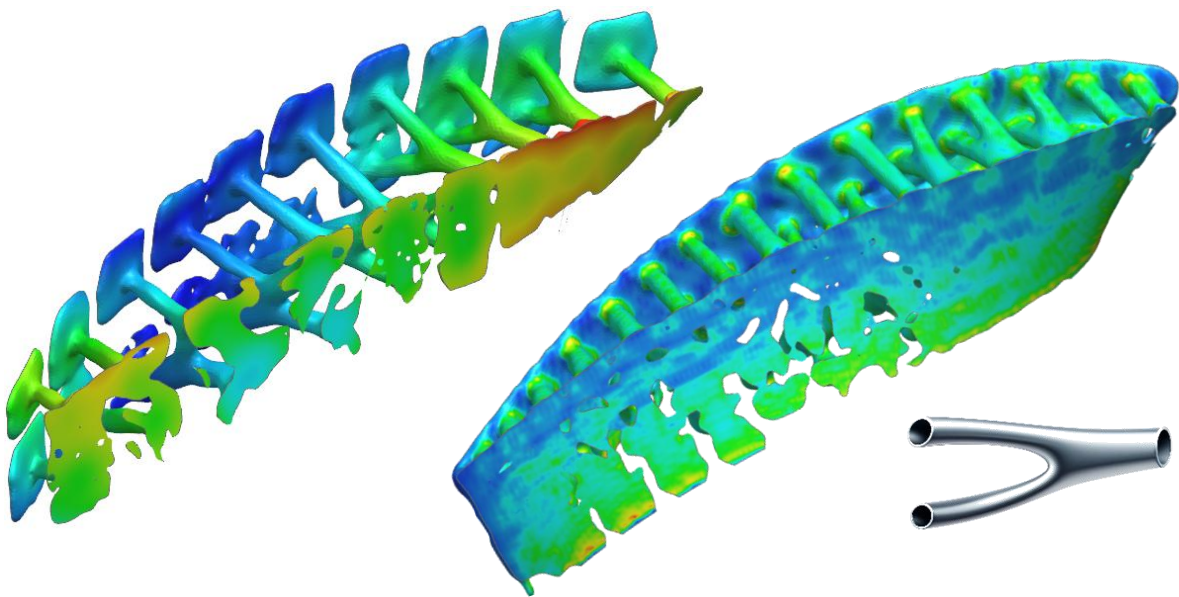
Figure 22 NX Topology Optimizer Results

4. MANUFACTURING CONSTRAINTS:

Although the Optimized solution is obtained while considering the main constraints but the main constraint here is the manufacturing constraint, which is defined by the technical capability of manufacturing equipment. As shown in Figure 23, the optimized solution consists of a branched structure, which is not feasible to manufacture within the propeller using the WAAM process. This type of structure can only be manufactured by the selective laser sintering (SLS) process.
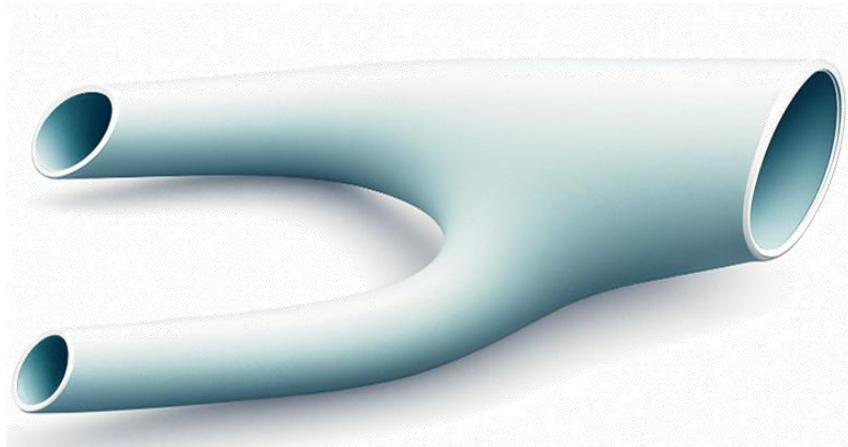
Figure 23 Internal Branch Structure

Therefore, two different simplified versions of this optimized solution are created, which are manufacturable by WAAM process.

4.1. Simplified versions of optimized solution:

Two different simplified versions of the optimized solution are as follows.

4.1.1. Straight bridge structure:

This version simplified the optimized solution by replacing the internal branches with a solid profile while keeping the number of supports as same and making the thickness of all supports constant along the whole section of profile. The 3D model of this simplified structure is shown below. The wall thickness of shell body is 10mm with an internal structure thickness of 8mm.
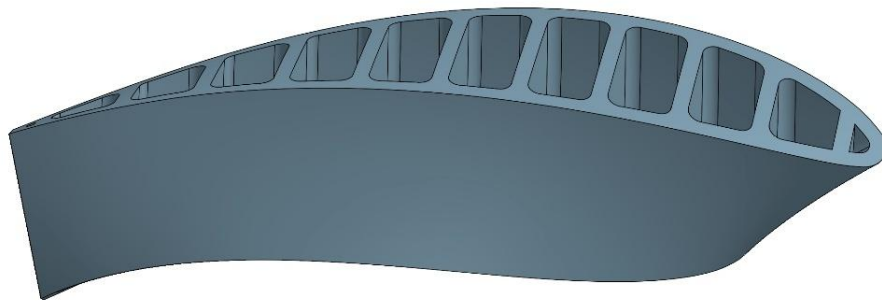
Figure 24 Simplified Straight Bridge support structure

4.1.2. Warren Truss structure:

This structure is assumed by converting the 3D branch structure as shown in Figure 23, into a 2D branch structure, which looks a lot like a Warren truss structure, but this structure has some unique characteristics, like the gap between the supports on the suction side is wider compared to the gap on pressure side, which is similar to the results of topology optimization as the stresses are higher at the pressure side due to higher pressure value. The structure is designed with a wall thickness of 10mm and internal structure with thickness of 8mm.
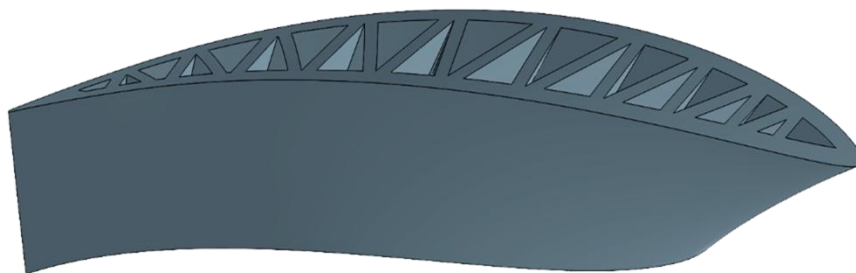
Figure 25 Blade section with Truss structure

5. BIO-INSPIRED PATTERN STRUCTURE

Throughout history, humans have looked to nature when searching for efficient and reliable design ideas. Biological structures, whether found in plants, animals, or microorganisms, have evolved through millions of years of adaptation and optimization, resulting in structural patterns that are not only strong but also lightweight and highly adaptable. This has led to growing interest in studying and applying similar principles to engineered systems.

The term "bio-inspired structures" refers to designs that involve taking cues from structures found in nature, like a honeycomb structure, how it balances strength and weight, or how the internal structure of our bones supports heavy loads without being totally solid. All these structures are result of adapting to their surrounding environment. These examples show that complex shapes can achieve impressive mechanical properties while staying lightweight. This approach has opened up possibilities in fields like aerospace, biomedical engineering, and additive manufacturing.

Figure 26 Water Lily Leaf Structure (Peng et al*., 2021), (b) Internal structure of bones (Microscopy of biology, no date) , (c) 3D printed parts inspired by lattice structure (*3D Printing Brings Water from Air - 3D Printing*, no date)*

One class of these structures that stands out is the so-called triply minimal surface geometries, which include forms like the gyroid. These continuous, 3D patterns don't repeat simply, but they manage to divide space very efficiently. They're increasingly seen as useful in areas where weight, strength, and material use need to be carefully balanced. In this context, the gyroid structure will be a central focus of this study. The evolution of gyroid structures is shown in Figure 27.
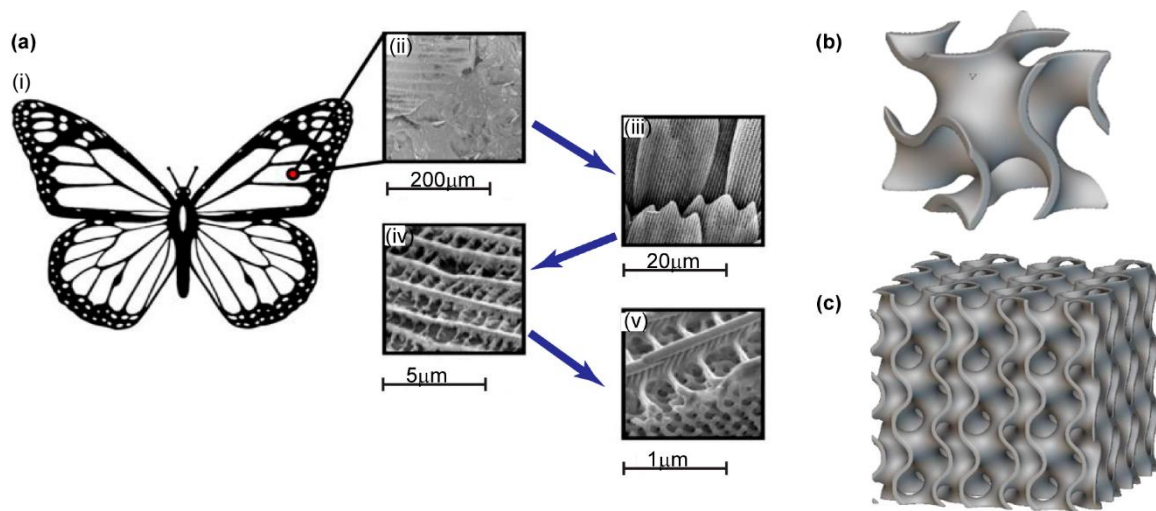
Figure 27 Inspiration of gyroid structure from Nature (Alemayehu and Todoh, 2024)

6. GYROID STRUCTURES:

The gyroid is remarkable among all the triply periodic minimum surfaces (TPMS) since it fills space continuously and splits it into two separate but interconnected volumes, despite not being self-intersecting and without mirror symmetry or straight lines. The gyroid surface is mathematically defined by the following equation.

$$\sin x \cos y + \sin y \cos z + \sin z \cos x = 0 \qquad (23)$$

This equation describes a surface in three-dimensional Cartesian space that is periodic along all three axes. It refers to a unit cell of side 2π, which is centered at the origin, as shown in Figure 28 (a), The element is a triangular surface, which is constructed by considering a basic element inside the octant identified by the length L/2.
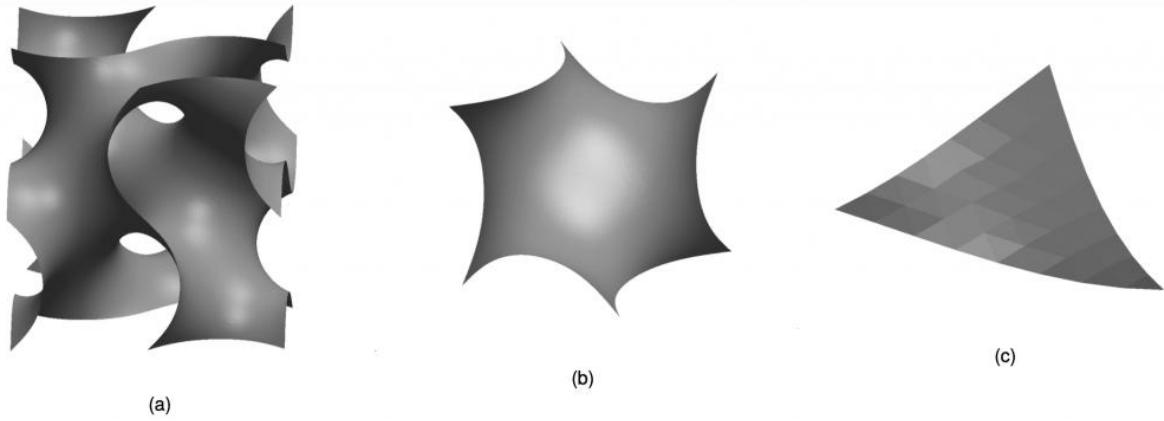
Figure 28 (a) Gyroid Element Cell, (b) Elemental octant, (c) Basic triperiodic element

The previous equation is particularized to the desired dimensions of the cell, which in this case is considered 5.

$$\sin\left(\frac{x-5}{L}2\pi\right)\cos\left(\frac{y-5}{L}2\pi\right) + \sin\left(\frac{y-5}{L}2\pi\right)\cos\left(\frac{z-5}{L}2\pi\right) + \sin\left(\frac{z-5}{L}2\pi\right)\cos\left(\frac{x-5}{L}2\pi\right) = 0 \ (24)$$

To identify the edges of the base element, the plane corresponding to one side of the cube is considered and solved in the two remaining variables.

$$\arctan\left[-\sin(x_i)\right] \ \& \ \arccos\left[-\cot(x_j)\right]$$

The variables x_i and x_j indicate the components in directions orthogonal to the plane considered. All 6 edges of the Octant surface can be described by rotating each component. Instead, considering the cell at distance $L / 4$, as shown in Figure 29, the origin is positioned in the middle of the octant, and to obtain the curve. Projection of the curves produced by intersecting

the frontal plane with the elementary cell on the edge (in red) and in the centre of the elementary octant (in blue) shown in Figure 29 (a) , and the Elementary octant with edge curves are shown in Figure 29 (b).

Figure 29 (a) Curves Projection, (b) Elementary octant
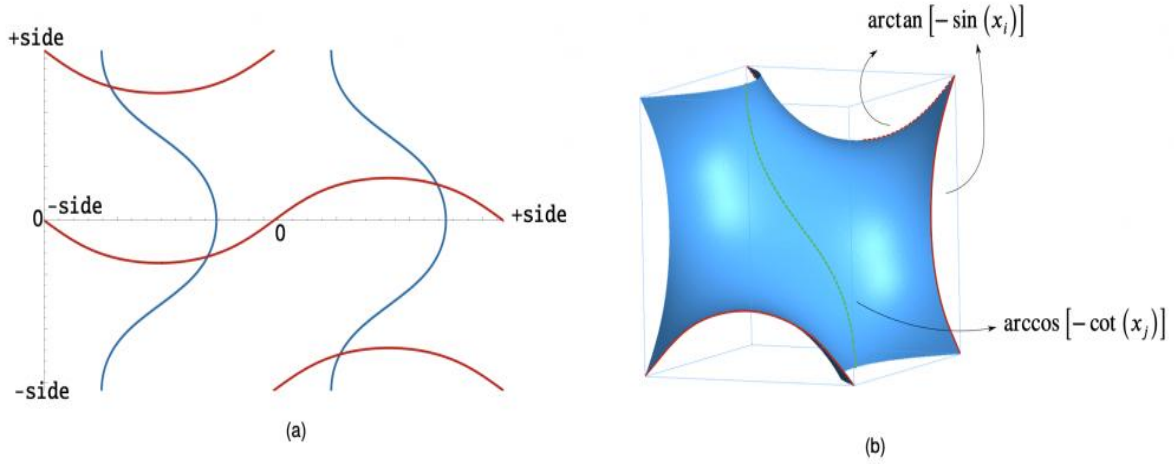
Unlike traditional lattice structures, the gyroid has no flat surfaces or sharp edges, which contributes to its remarkable mechanical and physical properties. Its constant curvature and smooth transitions between surfaces make it ideal for load distribution and energy absorption.

6.1. Structural Analysis for Propeller:

From a structural design standpoint, the gyroid is particularly interesting because it combines **lightweight characteristics** with **high stiffness** and **isotropic mechanical response**. These qualities make it an excellent candidate for applications where material efficiency is essential but structural integrity cannot be compromised. Unlike typical open-cell foams or truss-based lattices, the gyroid's continuous surface provides superior connectivity and stress distribution under mechanical loads.

For internal structure inside the propeller blade, gyroid structures offer an optimum strength-to-weight ratio. The gyroid is one of the greatest 3D infill patterns for additive manufacturing because it has the best strength-to-weight ratio, according to the paper's literature assessment and strength tests on several 3D lattices (Podroužek *et al.*, 2019). The following section discusses the findings of earlier research from the paper (Podroužek *et al.*, 2019).

In the referenced research that was conducted with a Polymer FDM 3D printer, several infill patterns were tested under compression to evaluate their mechanical performance. These consisted of complex 3D bio-inspired forms, such as the gyroid, Schwarz D, and Schwarz P triply surfaces, as well as more conventional 2D structures, like the hexagonal grid. Performance of these structures were evaluated in terms of weight, stiffness, and peak load for each construction, which was manufactured at three different scales.
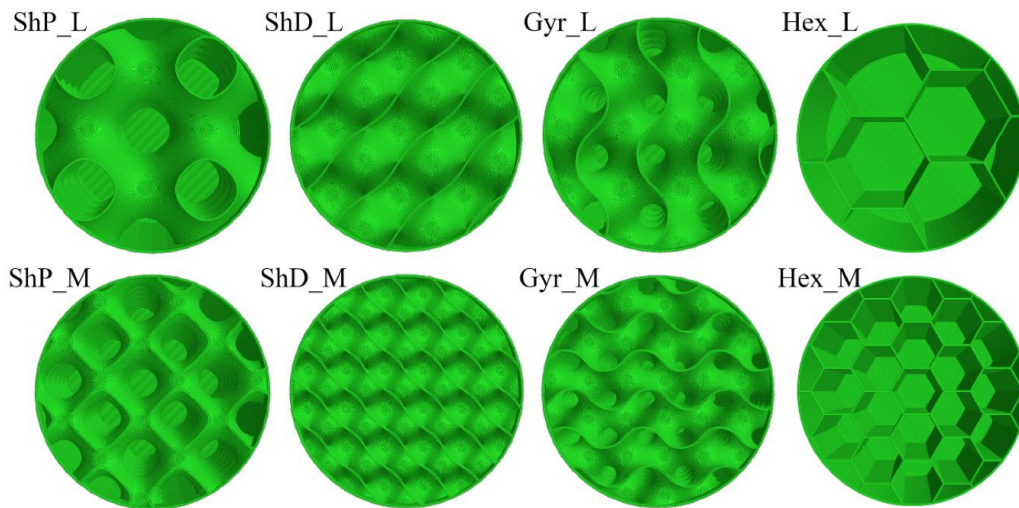
Figure 30 Overview of tested 3D and 2D infill alternatives (left to right): Schwarz P, Schwarz D, Gyroid (Podroužek et al.*, 2019)*

While the 2D hexagonal infill exhibited high stiffness and peak strength when the load direction was aligned with its internal structure, its performance significantly depended on orientation. This directional sensitivity, along with visible stress concentrations, limits its suitability for applications involving complex or curved geometries.

On the other hand, the 3D infill patterns showed a higher isotropic mechanical response, particularly the **gyroid** and **Schwarz D** structures. The gyroid, in particular, showed homogeneous stress distribution and less localized deformation due to its continuous curvature and lack of symmetry planes or straight lines. Due to these characteristics, components exposed to multidirectional forces, like marine propellers, experienced reduced premature buckling factors and increased ductility under compression. (Podroužek *et al.*, 2019)
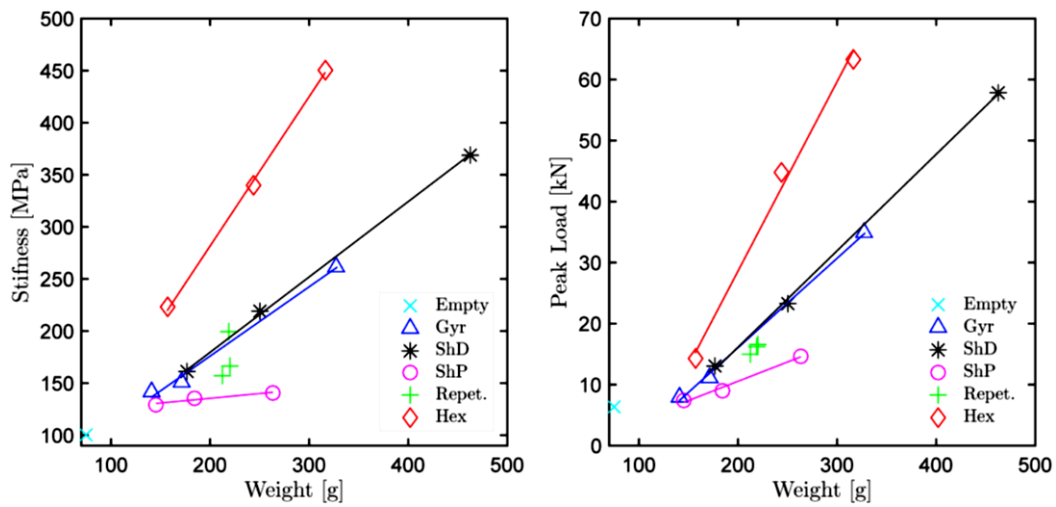
Figure 31 Stiffness and peak load comparison for 2D and 3D infill types (Podroužek et al.*, 2019)*

The gyroid's ability to maintain mechanical integrity while reducing weight makes it highly effective in situations where stress direction cannot be easily predicted. Additionally, it showed strong repeatability across specimens, confirming its reliability as a structural solution. Finite Element Analysis (FEA), calibrated using tensile tests with various slicing orientations, confirmed the gyroid's capability to distribute internal stresses uniformly.The efficacy of the gyroid structure for additive manufacturing applications involving complex loads is validated by the predicted strain fields, which, as seen in Figure 32, match the periodic patterns seen in physical experiments.
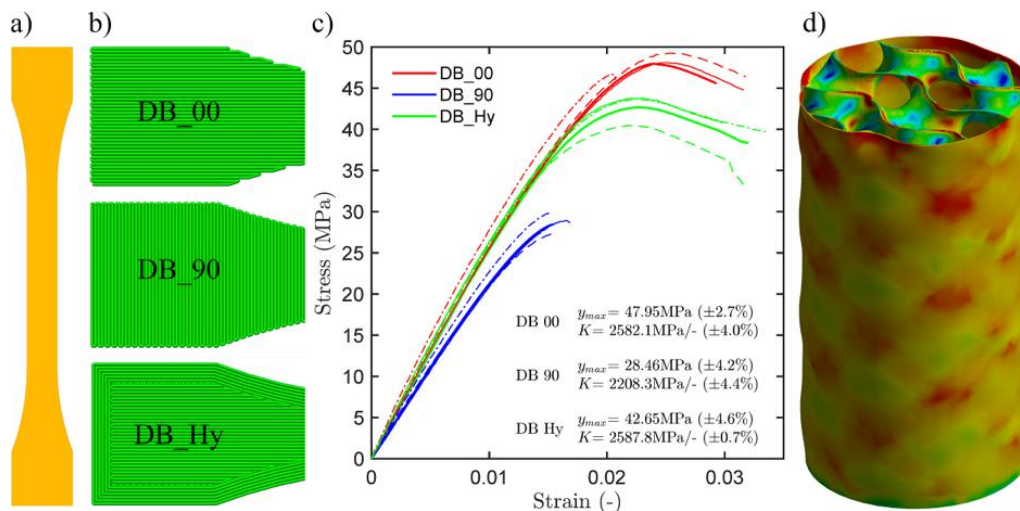
Figure 32 Influence of slicing strategy on tensile strength (left) and simulation of strain distribution in gyroid structure (right) (Podroužek et al.*, 2019)*

From a manufacturing perspective, its regular geometry allows for efficient layer-by-layer deposition in WAAM processes, without the need for internal support structures. Given all of these attributes, the gyroid structure is among the best options for the infill design of the propeller made using WAAM in this study.

6.2.Manufacturing Point of View:

Figure 33 3D-printing path simulation of gyroid structure

This page is left blank intensionally.

Chapter # 4

Result and Discussion

1. STRUCTURAL ANALYSIS OF THE BLADE SECTION WITH INTERNAL STRUCTURE:

For the Static Structure analysis, all three sections, including the solid section and two optimized sections with internal structures, are modeled and analyzed simultaneously. The details of the finite element analysis of the sections are as follows.

1.1. Assumptions in Boundary Conditions (for blade section):

In order to ensure numerical stability and realistically simulate the physical constraints, suitable boundary conditions were established at both R2 and R3

The truncated blade segment is treated as a standalone static model. In ANSYS Mechanical, fixed supports are commonly used to represent the effect of omitted geometry by "truncating the domain" (*Summary | ANSYS Boundary Conditions*, no date). Here, the inner (R2) face is an artificial boundary where the real blade would continue to the hub. As the blade root is rigidly attached to the hub, so the R2 face is constrained to prevent any motion. In practice, a remote support with all axis constraint at R2 locks all translational and rotational degrees of freedom on that face, effectively clamping the blade at R2. This method ensures that the segment behaves like a cantilevered slice of the blade, with no spurious rigid-body displacement. In ANSYS, applying appropriate supports is essential for a well-posed model without over-constraining it (*Summary | ANSYS Boundary Conditions*, no date) (*Boundary Conditions and Explanations in ANSYS - Mechead.com*, no date). By fixing only the R2 face (and not the free

blade surfaces), the model is fully constrained (preventing rigid-body modes) but not unduly stiffened.

In contrast, the outer (R3) face of the model is left traction-free (no imposed stresses). Since no symmetry or external structure is modeled beyond R3, this cut face carries no applied constraint. In linear elasticity, an unconstrained surface ("free" boundary) simply means zero traction (the stress vector normal to the surface is zero). Stated otherwise, only the applied suction or pressure on the blade sides drives the stress, allowing the R3 boundary to bend freely under internal pressure loads. R3 acts like a free edge since there is no displacement barrier (no sliding or fixed support) placed there. This choice is consistent with standard finite-element practice: when a physical boundary has no external loads or supports, it is treated as traction-free, allowing the internal stress field to develop naturally.

1.2. Finite Element Analysis of Different Blade Sections:

In this analysis, stress analysis is carried out on three different configurations of same blade section. The solid section, the simply supported section, and the truss support section. The detailed analysis is as follows.

1.2.1. Boundary conditions:

As previously defined, remote displacement is used at the bottom surface, and the top surface is free for all configurations. An example of remote displacement is shown in Figure 34.
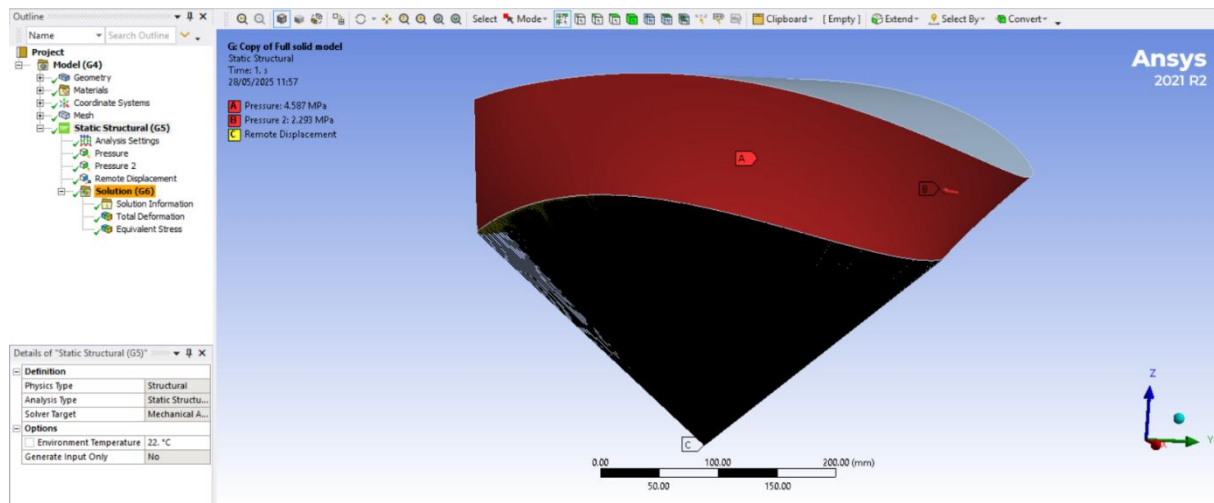
Figure 34 Remote displacement Boundary condition

While the pressure values are same as defined in Table 2.

1.2.2. Stress Analysis of full solid section:

After applying the boundary conditions, and defining the pressure at both the suction and pressure sides of the Blade. The Von Mises stresses are calculated, and the average stressed value is similar to the one compared in section 2.5.1, while the detailed stress profile is shown in Figure 35, which shows the average stress of 13.52 MPa, with a maximum stress of 33.39 MPa (while ignoring the singularity points). It is clear from the results that the maximum stress is far away from the maximum allowable limit of the material used.
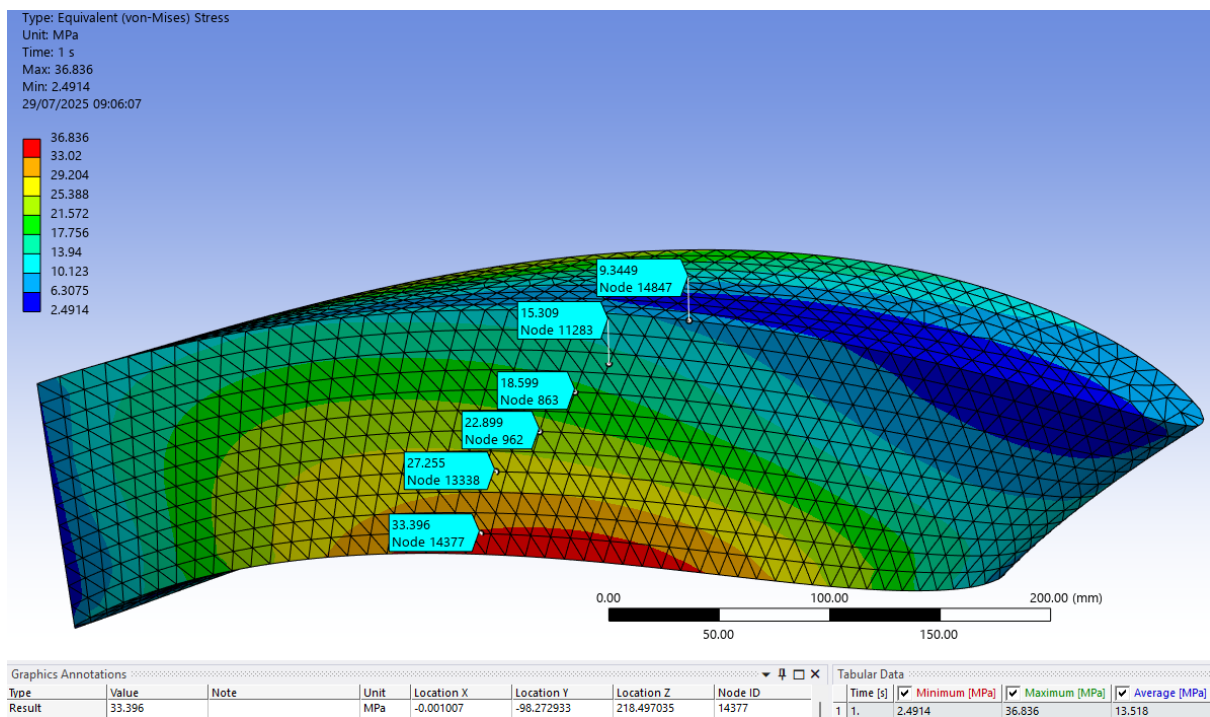
Figure 35 Stress result of Full solid Blade section
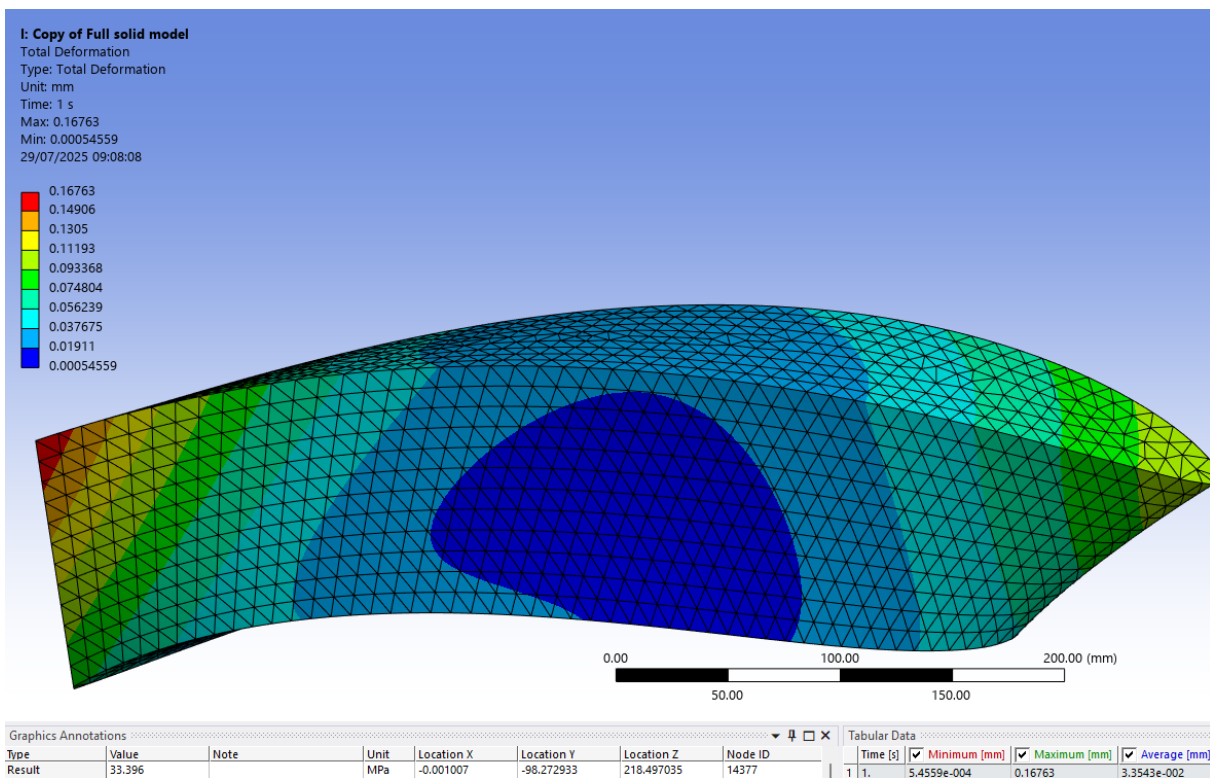
Figure 36 Deformation of full solid section

1.2.3. Stress Analysis of Straight bridge section:

The similar boundary conditions and pressure values are used for analyzing this section, and Von Mises stresses are calculated, and the average stress value comes to 41.613 MPa, as seen in Figure 37. The maximum stress value is very high due to the singularity points that are also marked in Figure 37. If these singularities are ignored, the highest value is around 63 MPa, which is within in safe limit of the material used.
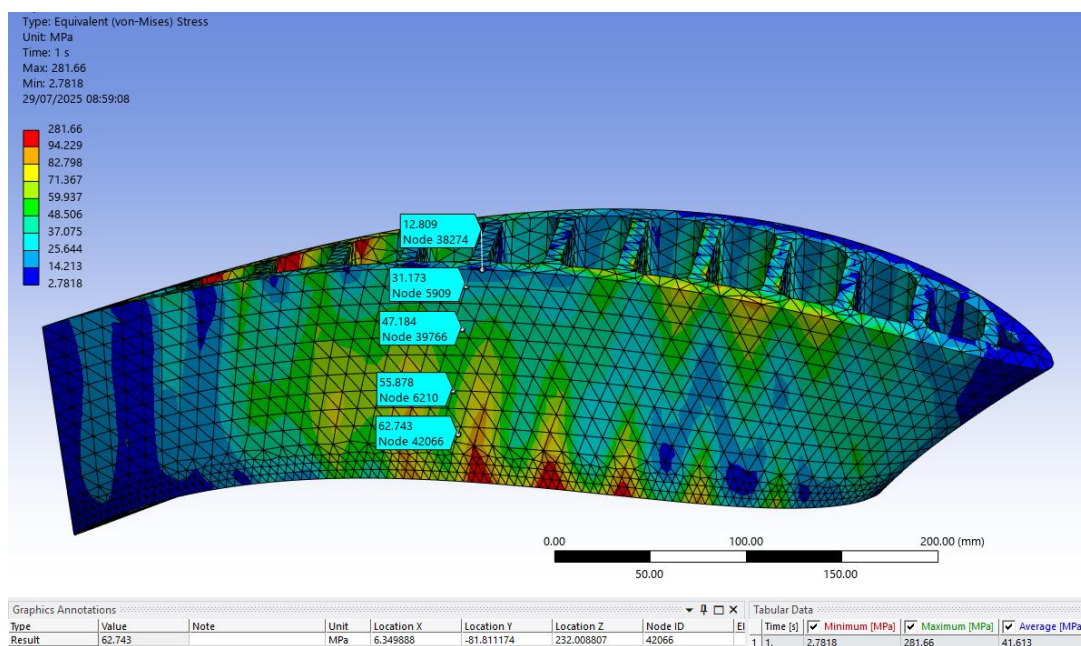
Figure 37 Stress result of Straight bridge Blade section
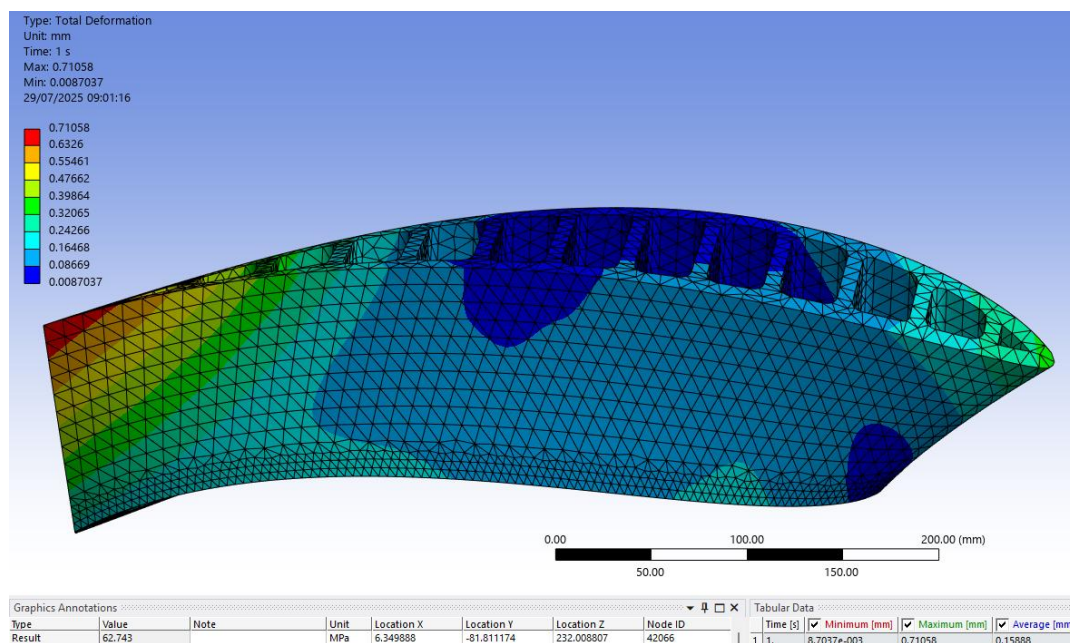
Figure 38 Deformation of Straight bridge section

1.2.4.   Stress Analysis of Truss Structure Section:

Similar to the last case, the same boundary conditions and pressure values are applied to this section. As shown in Figure 39, the average pressure value is 27.37 MPa, which is comparatively less than the straight bridge section. Similar to the other parts, there are some singularity points at bottom side of the model due to the boundary condition. If these singularities are ignored, the highest stress is around 54.14 MPa.
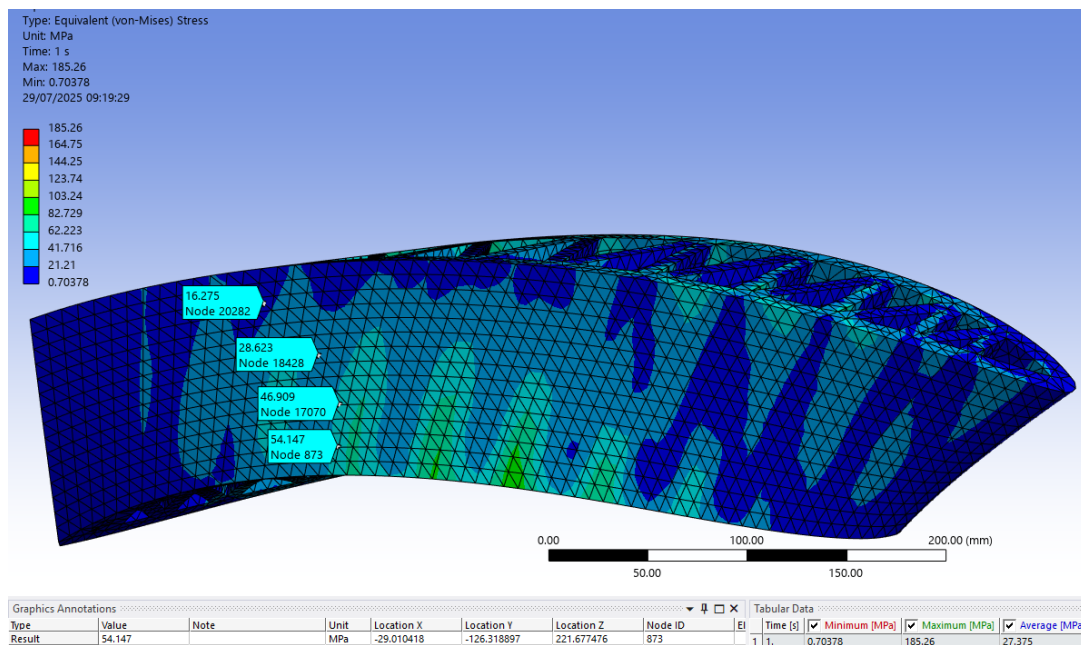
Figure 39 Stress result of Truss structured Blade section
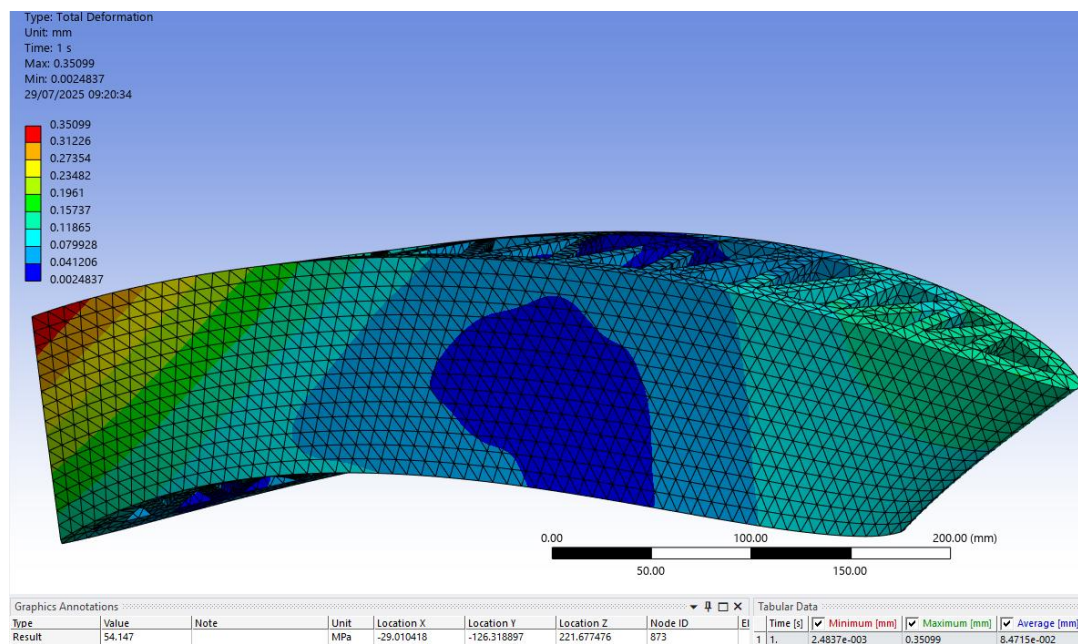
Figure 40 Deformation of straight bridge structure

1.3.Structure Analysis:

At first gyroid structure is created with optimum thickness and element radius, which are selected according to the blade dimensions and manufacturing limitations. The gyroid structure is shown in Figure 41.
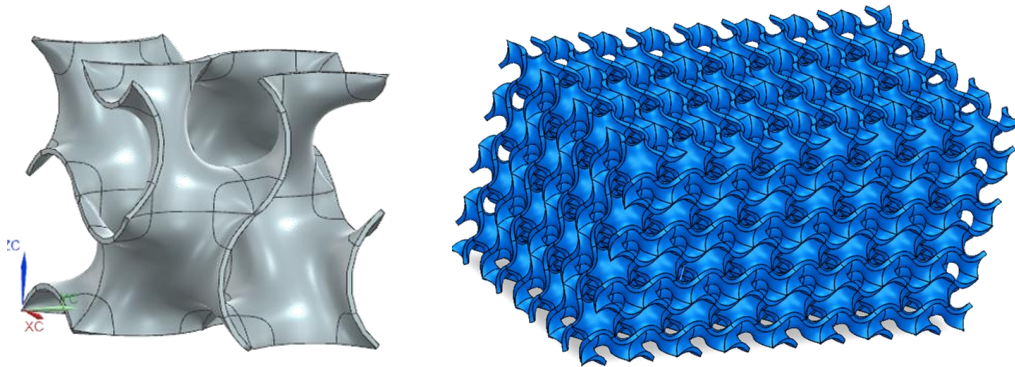
Figure 41 Gyroid structure 3D model

The gyroid structure, with a thickness of **5 mm**, is used for analysis, featuring an element radius of 30 mm. The structure is then transferred from R2 to R3 within the blade section to facilitate a proper comparison with other types of internal structures. The blade section with a gyroid structure is shown in Figure 41.
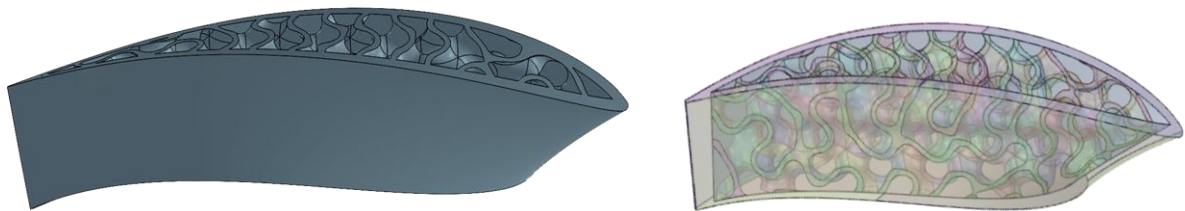
Figure 42 Blade section with Gyroid structure

After finalizing the CAD model, the section is then imported into ANSYS for structural analysis, and considering the complexity of internal structure, a fixed boundary condition is used at the bottom, while the pressure values are the same as those calculated in Table 2.

After applying the boundary conditions, Von Mises stress and deformation are calculated as shown in the figures below.

Figure 43 Von-Mises Stress on Gyroid section

Figure 44 Total Deformation on Gyroid Section

As shown in Figure 43, when high stress points due to singularity points (which are formed due to fixed boundary condition) are ignored, the maximum stress on the gyroid section is 43.97 MPa, while the average stress is around 22.57 MPa.

Table 3: Stress comparison in the blade section with different configurations

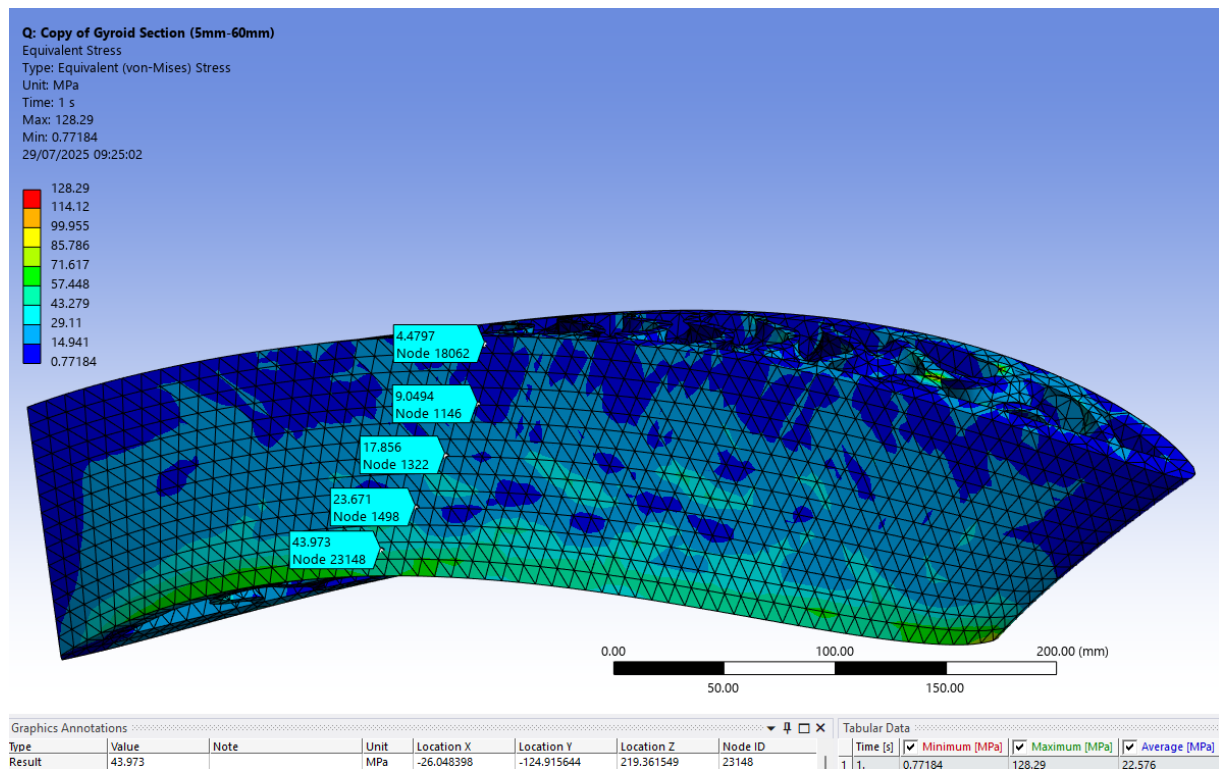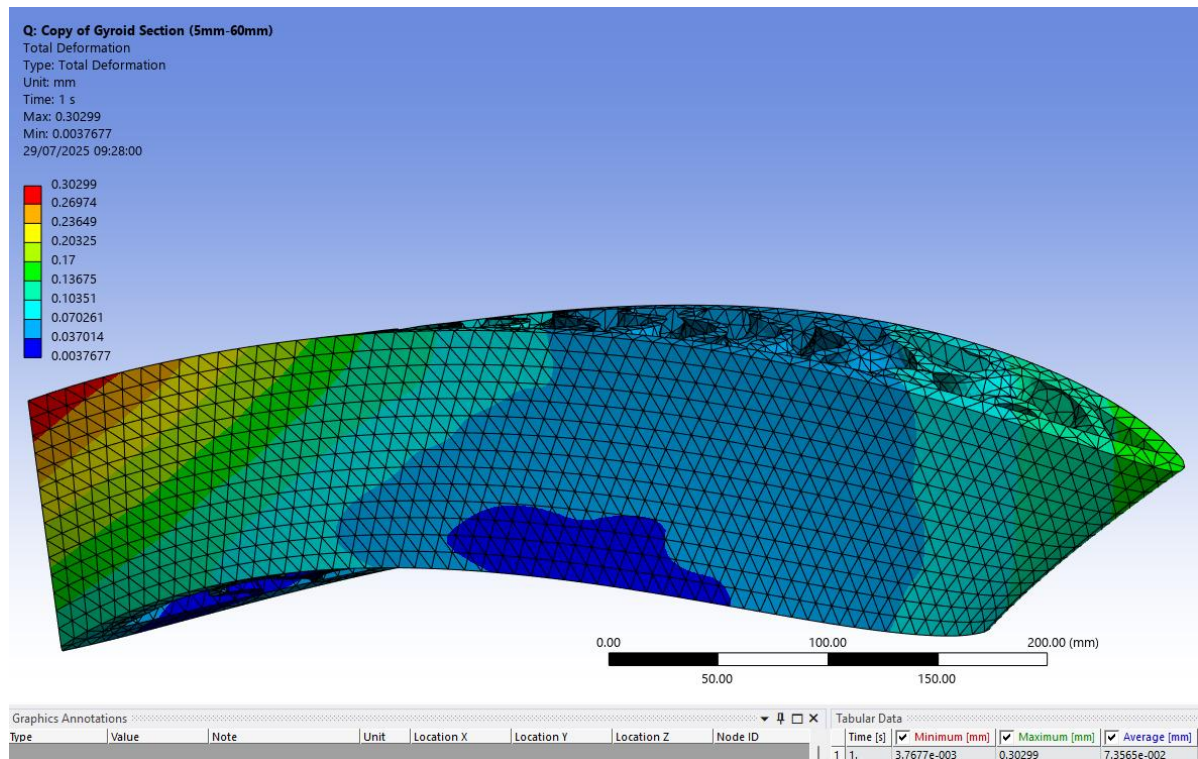| Stress comparison in different configurations (MPa)		
Configuration	**Average Stress**	**Maximum Stress**
Full solid Model	13.52	33.39
Straight bridge structure	41.61	62.74
Truss structure	27.37	54.15
Gyroid Structure	22.57	43.97

1.4. Discussion:

The stress analysis shows that the best configuration for the internal structure is a Gyroid structure. While considering that all structures have a higher wall thickness, and the internal structure of truss and straight bridge structure has a lower thickness than the wall, but compared to gyroid structure it's still higher, but still gyroid structure performs better because of its 3D geometric pattern, which leads to an average stress value of **22.57 MPa** with peak stress up to **43.97 MPa**. As this result shows that this type of structure is more feasible for the internal structure of the blade compared to other configurations, but as this structure is currently not possible to manufacture using current WAAM technology so the second best candidate is truss structure which has lower average and peak stress value as compared to straight bridge structure, coming at **27.37 MPa** and **54.15 MPa** respectivily. This truss structure is currently the best internal structure configuration because it can be manufactured using the technology currently in use.

2. STRESS ANALYSIS ON FULL BLADE:

After the initial analysis on the blade section, a proper detailed analysis is conducted on the full propeller blade geometry. Boundary conditions for this analysis are relatively simple, as the blade is fixed to the root and uniform pressure is applied on both sides of the blade, with different values for the pressure and suction sides as shown in Table 2.

2.1. Full solid body:

The static structural analysis on fully solid blade profiles how maximum stress is near the root of the blade from radius R 2.0 and R 3.0.
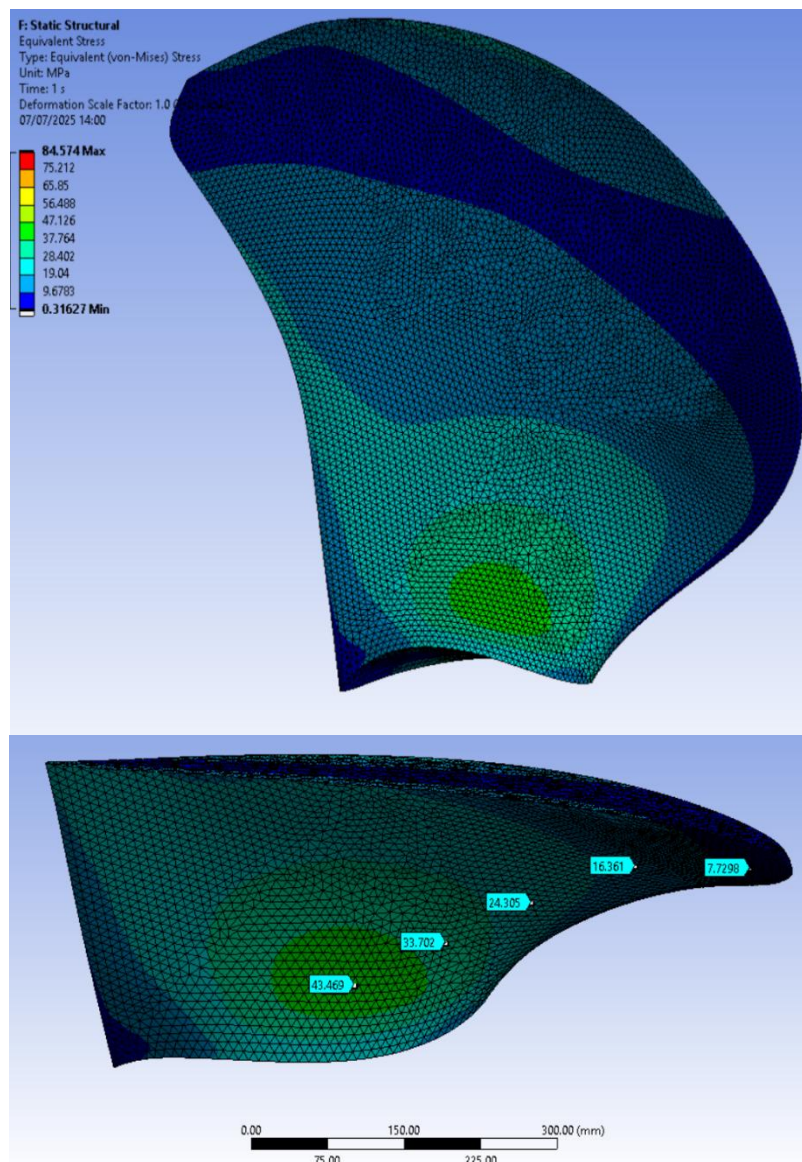
Figure 46 Von-Mises stress in Full solid blade

2.2. Straight Bridge Structure:

For this part, a full blade with an internal straight bridge structure is taken for FEM analysis to check the Von-Mises stress in the whole blade geometry. The results are as follows.
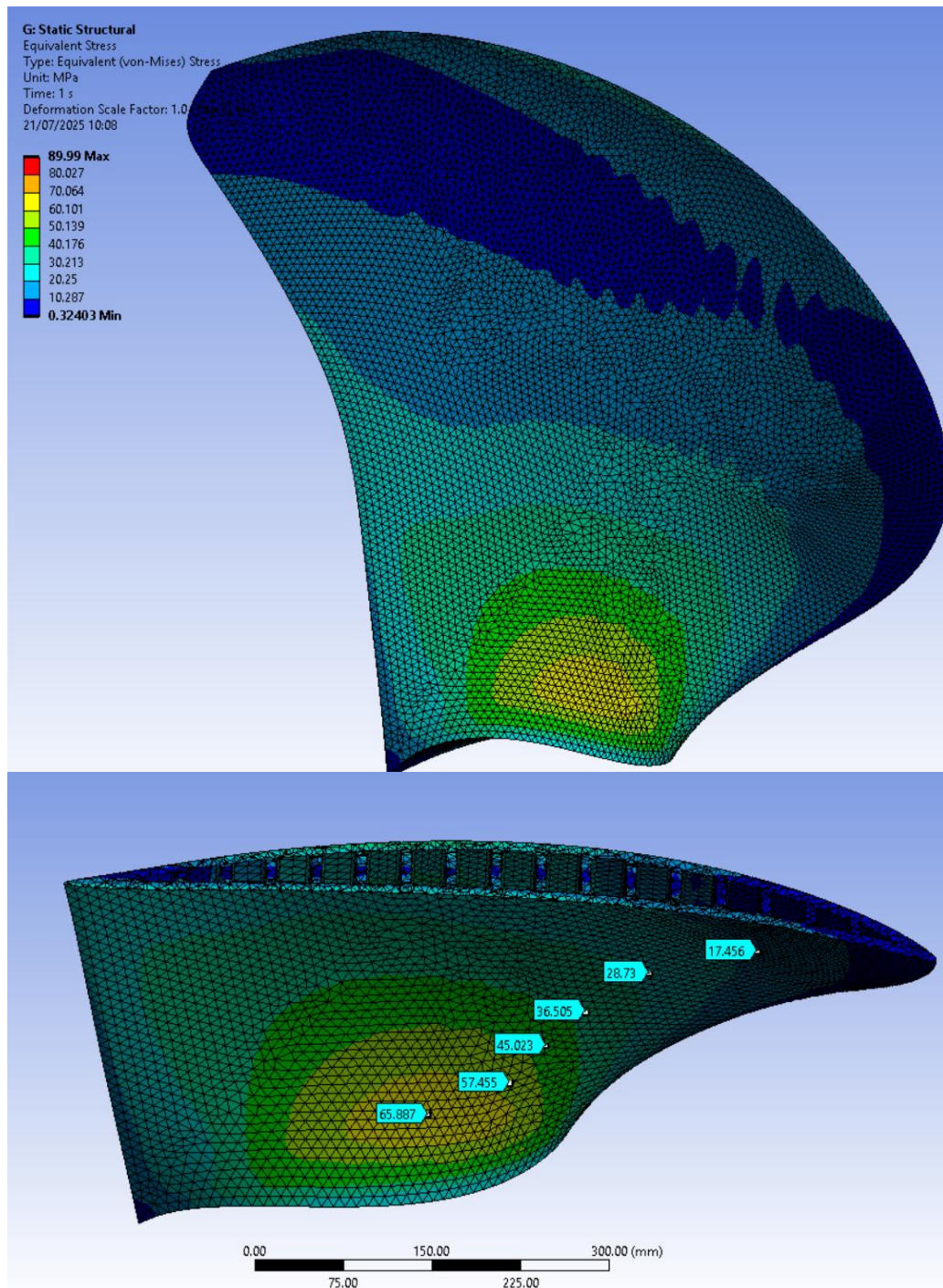

Figure 47 Von-Mises stress in Full Blade with Straight bridge structure

2.3. Blade with Truss Structure:

For this part, a full blade with internal truss structure is taken for FEM analysis to check the Von-Mises stress in the whole blade geometry. The results are as follows.
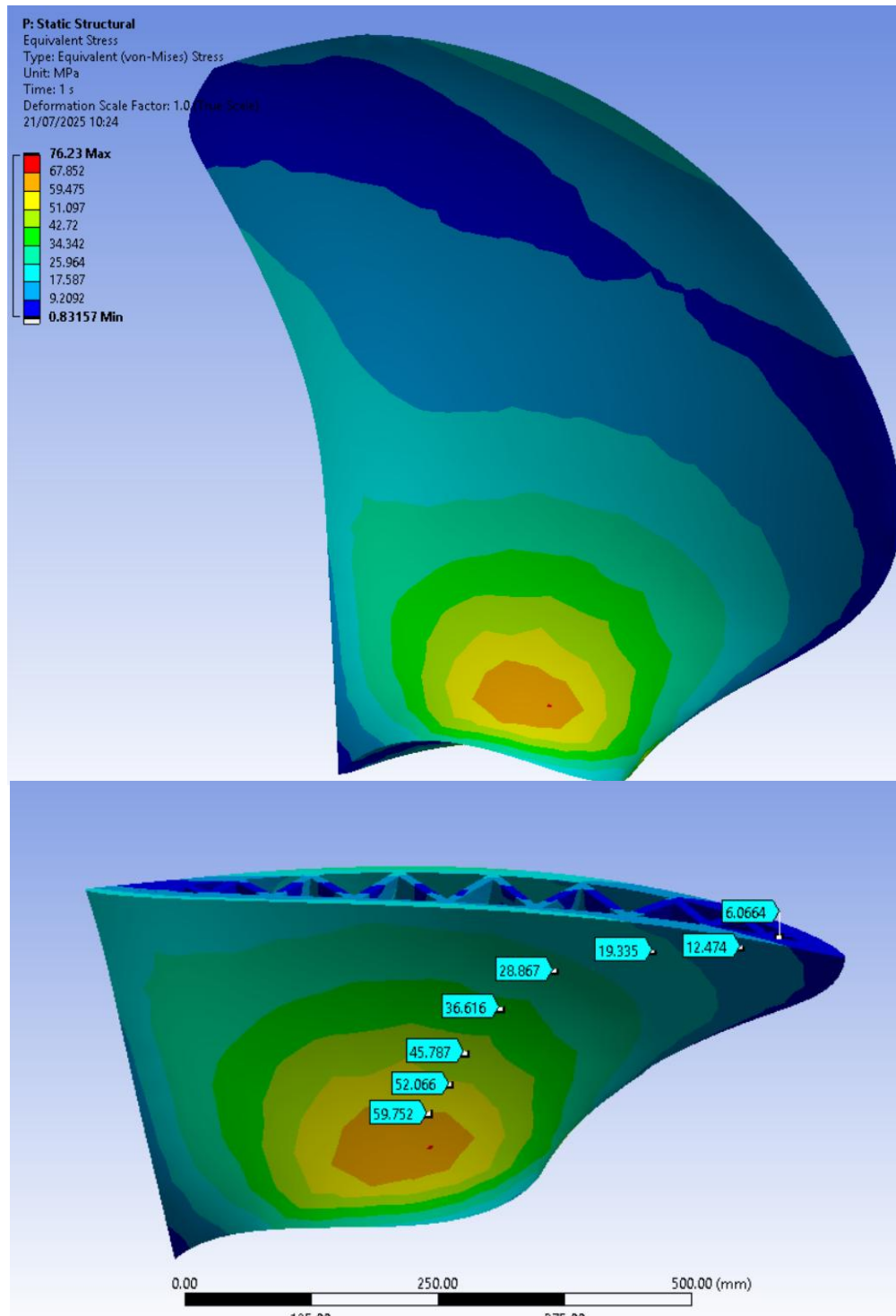
Figure 48 Von-Mises stress in Full Blade with Truss structure

Table 4: Stress comparison of full blade with different structural configurations.

Stress comparison in different configurations (MPa)		
Configuration	**Average Stress**	**Maximum Stress**
Full solid Model	10.9	43.5
Straight bridge structure	17.0	65.8
Truss structure	14.3	59.7
Gyroid Structure	---	---

The above results shown the maximum and average stress values which are considered after ignoring the stress concentration points caused by mesh irregularities, sharp corners, or boundary conditions, can produce artificially high values that are not representative of the overall structural behavior.

2.4. Volume Comparison:

The comparison of the total volume of different internal structure configurations (actual blade section) is shown in Table 5. The main to point to note here that all the structure has a wall thickness of 10mm while the Truss and straight bridge internal structure has thickness of 8mm, compare to 5mm for the gyroid structure.

Table 5: Density comparison of different internal structures

Configuration	Volume (mm^3)	Density (%)
Full solid	■■■■■■■	100
Straight bridge structure	■■■■■■■	More than 60-70%
Truss structure	■■■■■■■	More than 60-70%
Gyroid structure	■■■■■■■	45-65 %

As it's clear from Table 5 that the gyroid structure has a lower density compared to other structures, it provides better weight, material, and energy saving compared to any other internal structure.

2.5. Discussion:

As shown in Table 4, the stress value shows the same trend as analyzed in the blade sections. But the observed difference in stress values between the blade section and the full blade is primarily attributed to the variation in boundary conditions and model scope. The study in the blade portion (R2-R3), which uses a remote displacement boundary condition, focusses on a localised region with higher localised loading and curvature effects, leading in higher average stress levels.

In contrast, the full-blade model uses a Fixed Support boundary condition at the root (hub), introducing significantly higher restraints. The full blade exhibits higher maximum stress values because of strong constraint-induced bending and torsional loads concentrated near the blade root, even though localised stress concentrations were deliberately neglected during post-processing. This is because the overall volume contains low-stress areas (near the clamped root and blade tip), which lower the average stress:

- It includes the entire load path, from tip to hub, allowing full moment arm development.
- The fixed boundary condition creates a stiffer constraint, increasing internal load transfer and peak stress in regions near the root.
- Structural discontinuities near the hub as cross-section changes, which naturally result in higher stress levels.

As shown in Table 4, the truss structure exhibits lower stress values compared to the straight bridge structure; therefore, it is the best choice for the internal structure inside propeller blade.

The full blade with gyroid structure is not tested because of technical and time limitation.

Chapter # 5

Testing and Manufacturing Process

As the WAAM (Wire Arc Additive Manufacturing) process is used as the main manufacturing process, the setup is the same as discussed in Chapter 2, Section 4.

1. EQUIPMENT TESTING:

At first few tests have been conducted to understand the manufacturing capability of the setup fully. These tests are conducted mainly with two materials, Aluminum-Bronze and Stainless steel. In order to determine the ideal printing parameters, the settings for voltage, current, and other welding factors were adjusted during several tests.

1.1.Inclination Test:

Figure 49 Inclination test using WAAM

1.2. Bending Test:
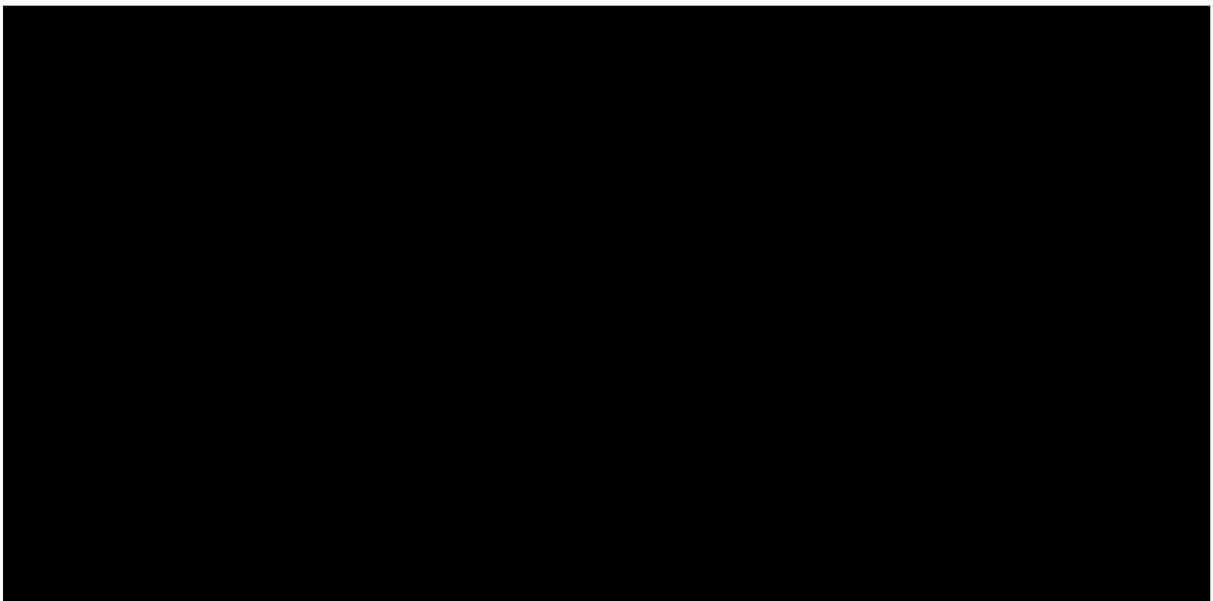
Figure 50 Three point bending test
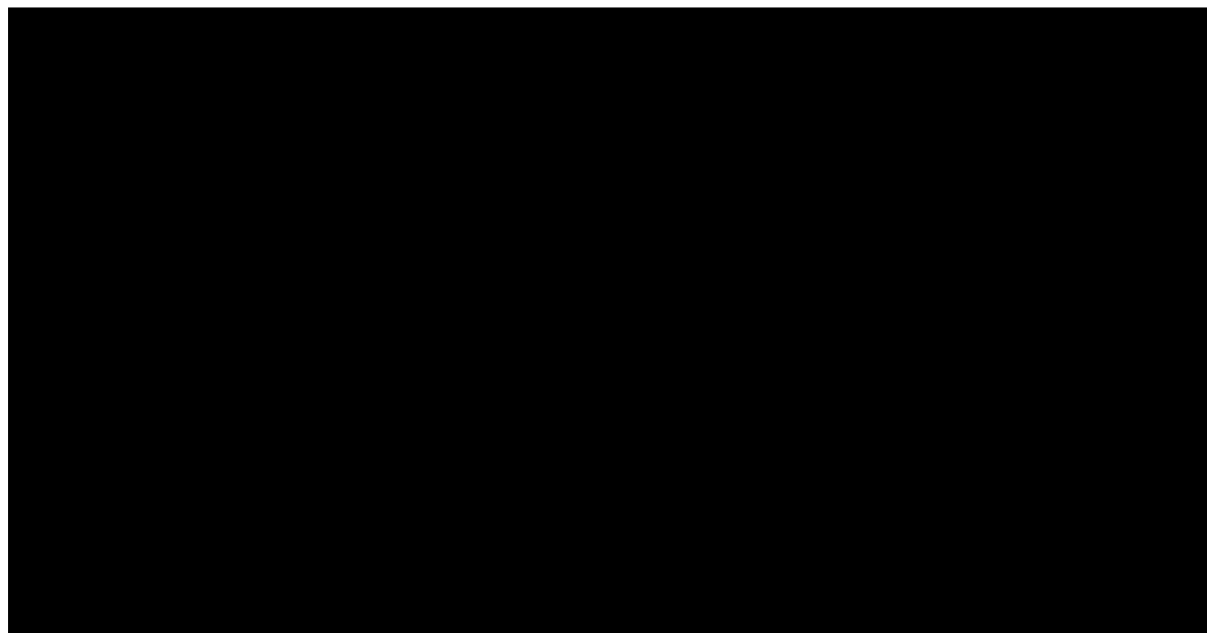
Graph 6 Three point Bending test
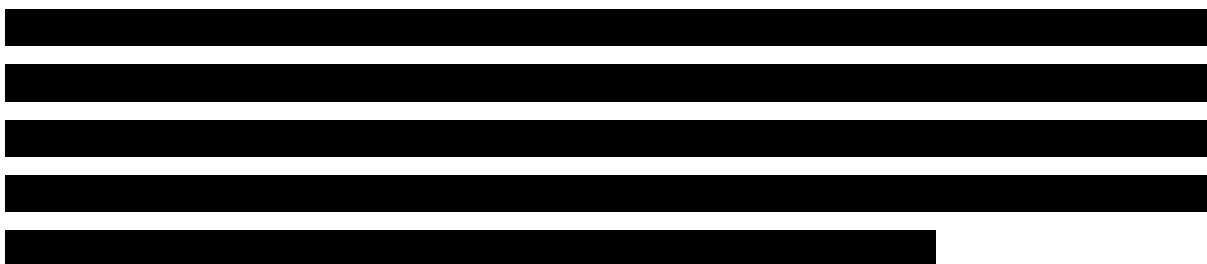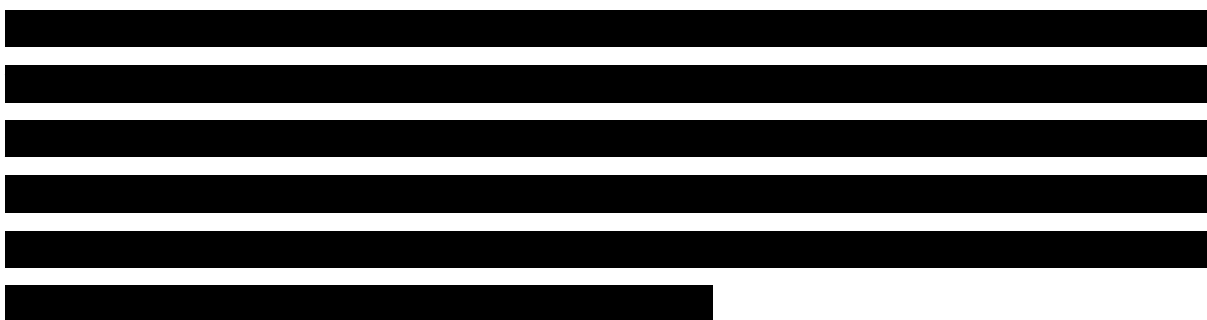
1.3. Tensile testing:

██

██

██

██

██

██

██

██

██

██

███

██
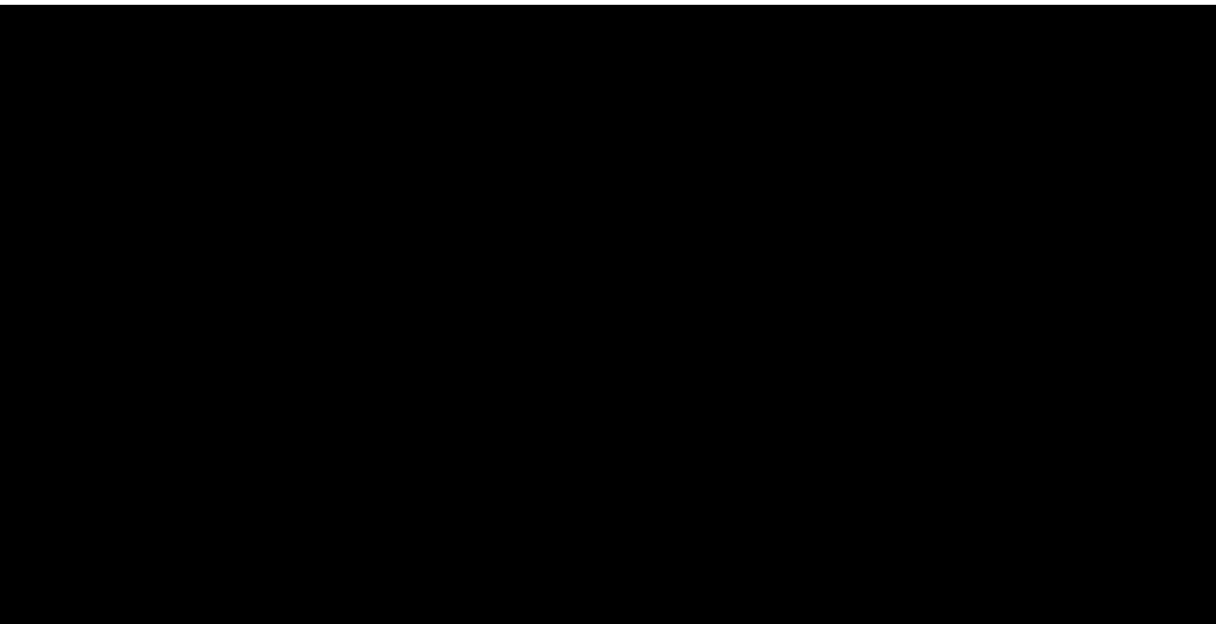
Graph 7 Tensile testing of WAAM component.

██

██

███

2. PREVIOUSLY MANUFACTURED MODELS:

As part of a past study, some 3D-printed propeller models were manufactured. Some of these models are then compared with the casted propellers. One such model is shown in Figure 51.

Figure 51 Comparison of 3D printed and casted propeller

 As shown in Figure 51, the 3D-printed propeller has a patterned surface, which is then smoothed with CNC milling to achieve a smooth surface finish, as illustrated in Figure 52. The final version of the 3D-printed propeller has a superior surface finish compared to the cast one.

Figure 52 3D -printed Propeller with one side milled.

3. 3D-PRINTED BLADE SECTION WITH DIFFERENT INTERNAL STRUCTURES:

All three types of internal structures investigated in this research are initially manufactured with a polymer 3D-printer to evaluate the printing path, dimensional accuracy, and analyze the overall internal structure. These prototypes are created on 18% of the actual scale of the propeller blade.

Figure 53: 3D-printed prototypes of blade section with different internal structures

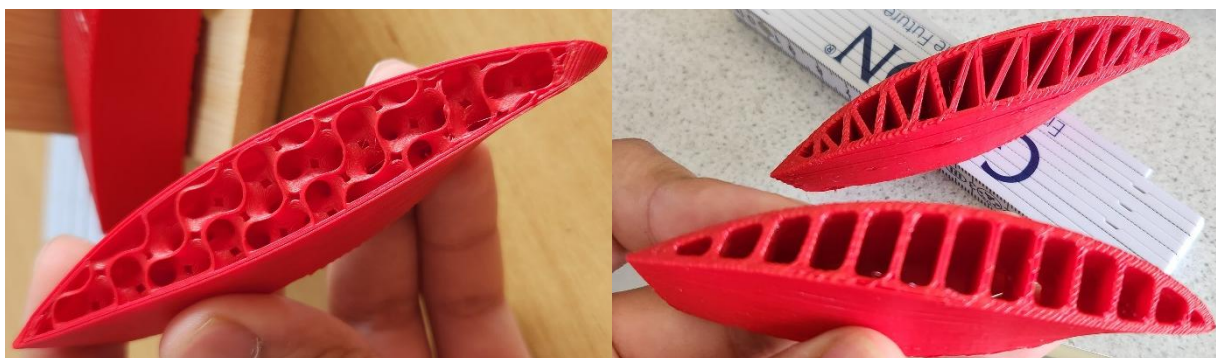As shown in Figure 53, the internal structures fill the blade profile perfectly, and all the details are still visible in case of gyroid structure. Along with these smaller prototypes, a larger-scale model was also developed using the large-scale polymer 3D printer to adjust and visualize the printing path. The scaled model is shown in Figure 54.

*Figure 54 Scaled prototype of propeller section with gyroid structure*

Along with manufacturing plastic models, the company is currently working on path optimization to create a scaled model from metal 3D printing using WAAM. Which will help to understand the manufacturing process of larger-scale propeller blades and to study any defects and issues encountered during the manufacturing of these complex internal structures.

Conclusion:

This study and research set out to develop and evaluate internal structures for additively manufactured marine propeller blades, intending to reduce material usage, cut production time, along with time and weight savings while maintaining structural integrity under service loads. Three distinct patterns were conceptualized and incorporated within a standard propeller geometry. The first study involved a topology optimization with concluded with a branch structure inside blade geometry, which was simplified into two different internal structure configurations due to manufacturing technology limitations. This results in a truss-based and a straight-bridge internal structure. On the other hand, a biomimetic gyroid design configuration was studied and chosen for further analysis. Each design was tailored to fit the blade's complex contours and was subjected to comprehensive finite-element analysis in ANSYS to assess stress distribution, deformation characteristics, and overall stiffness-to-mass performance.

██
██
██
██
██
██
██
██
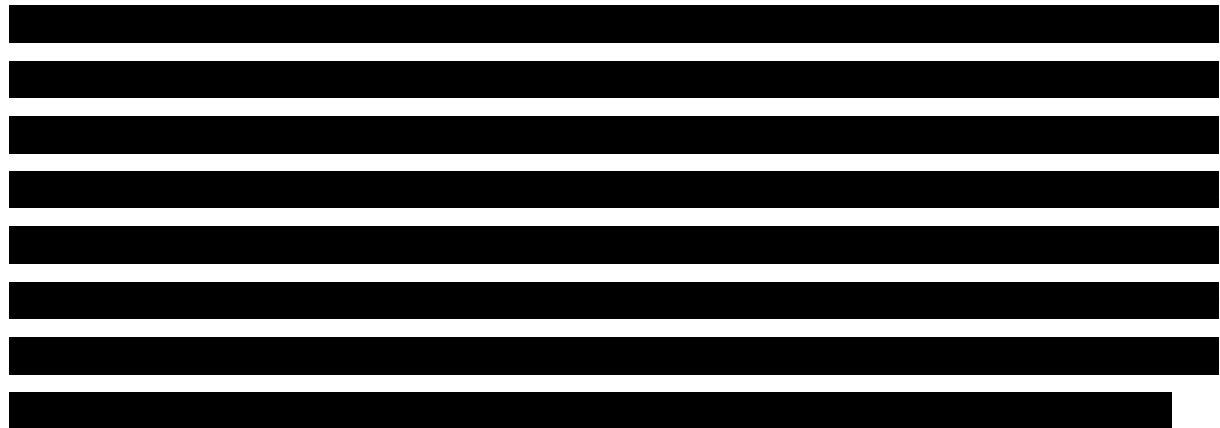
While the gyroid configuration represents an ideal solution from a performance standpoint, current limitations of wire-arc additive processes render its realization challenging. The other limitation of this complex structure includes, requirement for a high-end computation system for the design and structural analysis of a propeller blade with internal gyroid structure. However, the gyroid structure is in current interest, and engineers at MMG have started to make this complicated structure feasible to manufacture using existing WAAM technology. This will require some modifications or adjustments to the current equipment and manufacturing parameters, as well as path optimization, so that gyroid-based blades may be practically fabricated soon.

██
██

██

██

██

████████████████████████

Ultimately, this work demonstrates the potential of topology-driven and bio-inspired internal architectures to revolutionize propeller manufacturing. By integrating advanced computational design with practical Additive Manufacturing constraints, it lays a foundation for lightweight, high-performance marine propulsion components. Future research will focus on refining deposition strategies, improving surface finish, and validating prototype blades in operational sea trials, with a view to fully harnessing the advantages of gyroid structures once manufacturing technologies mature.

This page is left blank intensionally.

4. REFERENCES

3D Printing Brings Water from Air - 3D Printing (no date). Available at: https://3dprinting.com/military/3d-printing-brings-water-from-air/ (Accessed: 16 June 2025).

Alemayehu, D.B. and Todoh, M. (2024) 'Enhanced Energy Absorption in Bioinspired Combined TPMS-Gyroid and Walled TPMS-Gyroid Lattice Structure Manufactured via Fused Filament Fabrication (FFF)'. Available at: https://doi.org/10.20944/PREPRINTS202403.1003.V1.

Basic Principles of Ship Propulsion, MAN Diesel & Turbo. (no date). Available at: https://www.man-es.com/docs/default-source/document-sync/basic-principles-of-ship-propulsion-eng.pdf (Accessed: 6 May 2025).

basis-propulsion.pdf (no date). Available at: https://www.slideshare.net/slideshow/basispropulsionpdf/255683145 (Accessed: 20 March 2025).

Boundary Conditions and Explanations in ANSYS - Mechead.com (no date). Available at: https://www.mechead.com/boundary-conditions-and-explanations-in-ansys/ (Accessed: 20 May 2025).

Göttsche, U. *et al.* (2024) 'Hybrid manufacturing of a hollow ship's propeller : investigation from material characterization to implementation', pp. 737–746. Available at: https://doi.org/10.15480/882.9360.

Kornev, N. (2019) *Lectures on ship manoeuvrability*. 1st edn.

Peng, X. *et al.* (2021) 'Design and Simulation of Sandwich Structure of Exoskeleton Backplate Based on Biological Inspiration', *Journal of Physics: Conference Series*, 1885(5). Available at: https://doi.org/10.1088/1742-6596/1885/5/052066.

Podroužek, J. *et al.* (2019) 'Bio-inspired 3D infill patterns for additive manufacturing and structural applications', *Materials*, 12(3). Available at: https://doi.org/10.3390/MA12030499

Summary / ANSYS Boundary Conditions (no date). Available at: https://innovationspace.ansys.com/courses/courses/structural-boundary-conditions/lessons/summary-20/?template=rocky (Accessed: 20 May 2025).

(No date) 'Microscopy of Biological Materials for Bioinspired Design | ZEISS'. Available at: https://www.zeiss.com/microscopy/en/resources/insights-hub/materials-sciences/microscopy-of-biological-materials-for-bioinspired-design.html (Accessed: 16 June 2025).

Other documents used in research, referred to DNV regulations, can not be included in references because of the confidentiality of documents, although references to the specific chapters and sections are mentioned in the main body.

5. APPENDIX

WAAM process setup.